JCI insight

Lysosomal acid lipase, CSF1R and PD-L1 determine functions of CD11c+ myeloid-derived suppressor cells

Ting Zhao, … , Hong Du, Cong Yan

JCI Insight. 2022. https://doi.org/10.1172/jci.insight.156623.

Research In-Press Preview Immunology

Graphical abstract

Lysosomal Acid Lipase, CSF1R and PD-L1 Determine Functions of CD11c$^+$ Myeloid-Derived Suppressor Cells

Ting Zhao,[1] Sheng Liu,[2,3] Xinchun Ding,[1] Erica M. Johnson,[1] Nasser H. Hanna,[2] Kanhaiya Singh,[4] Chandan K Sen,[4] Jun Wan,[2,3] Hong Du,[1,2] and Cong Yan [1,2]

[1]Department of Pathology and Laboratory Medicine, Indiana University School of Medicine, Indianapolis, Indiana, USA

[2]IU Simon Comprehensive Cancer Center, Indiana University School of Medicine, Indianapolis, Indiana, USA

[3]Department of Medical and Molecular Genetics, Indiana University School of Medicine, Indianapolis, Indiana, USA

[4]Indiana Center for Regenerative Medicine and Engineering, Indiana University School of Medicine, Indianapolis, Indiana, USA

The authors have declared that no conflict of interest exists.

Correspondence: Dr. Cong Yan, Department of Pathology and Laboratory Medicine, Indiana University School of Medicine, 975 W Walnut Street, IB424G, Indianapolis, IN 46202. E-mail: coyan@iupui.edu. Tel: 1-317-278-6005; or Dr. Hong Du, Department of Pathology and Laboratory Medicine, Indiana University School of Medicine, 975 W Walnut Street, IB424E, Indianapolis, IN 46202. E-mail: hongdu@iupui.edu. Tel: 1-317-274-6535.

Abstract

Lysosomal acid lipase (LAL) is a key enzyme in the metabolic pathway of neutral lipids. In the blood of LAL deficient (*Lal*$^{-/-}$) mice, increased CD11c^{+} cells were accompanied by up-regulated PD-L1 expression. Single cell RNA sequencing of *Lal*$^{-/-}$ CD11c^{+} cells identified two distinctive clusters with a major metabolic shift towards glucose utilization and reactive oxygen species (ROS) over-production. Pharmacologically blocking pyruvate dehydrogenase in glycolysis not only reduced CD11c^{+} cells and their PD-L1 expression, but also reversed their capabilities of T cell suppression and tumor growth stimulation. Colony-stimulating factor 1 receptor (CSF1R) plays an essential role in controlling *Lal*$^{-/-}$ CD11c^{+} cell homeostasis and function and PD-L1 expression. Inhibition of LAL activity by pharmacological inhibitor increased CD11c, PD-L1 and CSF1R levels in both normal murine myeloid cells and human blood cells. Tumor-bearing mice and human non-small-cell lung cancer (NSCLC) patients also showed CD11c^{+} cell expansion with PD-L1 and CSF1R up-regulation and immunosuppression. There were positive correlations among CD11c, PD-L1 and CSF1R expression and negative correlations with LAL expression in lung cancer and melanoma patients using the TCGA database and patient samples. Therefore, CD11c^{+} cells switched their functions to immune suppression and tumor growth stimulation through CSF1R/PD-L1 upregulation and metabolic reprogramming.

Keywords: CD11c^{+} cells, lysosomal acid lipase, single cell RNA sequencing, metabolic reprograming, CSF1R, PD-L1, lung cancer, melanoma

Introduction

Immune cells in the tumor microenvironment actively participate in cancer initiation, progression and metastasis (1). Thus, interactions between immune cells and tumor cells determine the balance between immunity and tolerance to tumor cells. The signaling pathway of programmed death-ligand 1 (PD-L1, B7-H1 or CD274) and its receptor PD-1 (CD279) is an important mechanism utilized by tumors to escape antitumor immune responses (2, 3), and maintain an immunosuppressive state in the tumor environment (4). PD-L1 binds to PD-1 or CD80 (B7-1) on activated T cells to mediate an inhibitory signal, and to prevent the immune system from rejecting the tumor (5, 6). Antibody-based therapeutics targeting PD-L1 have shown clinical responses in multiple tumor types (7, 8). PD-L1 is broadly expressed in hematopoietic cells, including dendritic cells (DCs) (9). Blockade of PD-L1 on DCs has been reported to enhance T cell activation and cytokine production (10). However, it is still not entirely clear how PD-L1 expression is regulated in immune cells to affect tumor progression. DCs are a diverse group of specialized antigen-presenting cells (APCs) with key roles in the initiation and regulation of innate and adaptive immune responses. Much interest in modulating DC function has been given to cancer immunotherapy by generations of DC-based vaccines (11-13). Most DCs express CD11c as a surface marker (12, 14). The diversity and functions of $CD11c^+$ cell subsets that are shaped by pathogenic conditions are not completely understood, especially those $CD11c^+$ cells that tolerate and stimulate cancer growth.

Lysosomal acid lipase (LAL) is a key enzyme in the metabolic pathway of neutral lipids, which hydrolyzes cholesteryl esters and triglycerides in the lysosome of cells to generate free fatty acids and cholesterol. Clinical case reports indicated that mutations

of the LAL gene were associated with carcinogenesis in patients (15). In LAL knockout (*Lal*$^{-/-}$) mice, myeloid populations systemically expand from hematopoietic progenitors in the bone marrow, suppress T cell proliferation and function, and stimulate tumor growth and invasion in both syngeneic and allogeneic backgrounds (16-18). The LAL deficiency-induced immunocompromise also allows growth of human cancer cells in mice (19).

The present study found that LAL deficiency in the *Lal*$^{-/-}$ mouse model increased the CD11c^{+} cell population in the blood that was associated with up-regulation of PD-L1 expression. These *Lal*$^{-/-}$ CD11c^{+} cells shared characteristics of myeloid-derived suppressor cells (MDSCs) by suppressing T cells and stimulating tumor growth. Single cell RNA sequencing (scRNA-seq) analysis identified two distinct clusters with differential gene expression patterns, and revealed a major metabolic shift towards glucose utilization and reactive oxygen species (ROS) over-production in *Lal*$^{-/-}$ CD11c^{+} cells. Colony-stimulating factor 1 receptor (CSF1R) has been identified as a gateway keeper in controlling *Lal*$^{-/-}$ CD11c^{+} cell homeostasis and functions. Findings discovered in CD11c^{+} cells of *Lal*$^{-/-}$ mice were also reproduced in CD11c^{+} cells of tumor-bearing mice and human cancer patients. In humans, there were positive correlations among *CD11C*, *CD274* (PD-L1), *CSF1R* and *IFNG* (IFNγ) expression and negative correlations with *LIPA* (LAL) expression in multiple cancer forms using The Cancer Genome Atlas (TCGA) database. Human non-small-cell lung cancer (NSCLC) patients showed CD11c^{+} cell expansion with PD-L1 and CSF1R up-regulation and decreased LAL expression in their blood. These studies demonstrate that in addition to their APC function, CD11c^{+} cells are able to switch to subpopulations that exhibit immune suppression and tumor growth stimulation in the

tumor environment as a result of metabolic reprogramming, and PD-L1 and CSF1R up-regulation.

Results

Increase of PD-L1 expression in *Lal*$^{-/-}$ CD11c^{+} cells.

The percentage of PD-L1^{+} cells in the whole blood was increased in *Lal*$^{-/-}$ mice vs. *Lal*$^{+/+}$ mice (Figure 1A and Supplemental Figure 1A). Since T cells in the blood of *Lal*$^{-/-}$ mice were dramatically reduced compared with those of *Lal*$^{+/+}$ mice (20), it is unlikely that the T cells are responsible for the increase of PD-L1 expression. To further assess which cell population in the myeloid component is responsible for the increase of PD-L1 expression, the PD-L1 level in various myeloid cell subtypes was analyzed by flow cytometry. Compared with *Lal*$^{+/+}$ mice, PD-L1 expression was up-regulated in CD11c^{+}, MHCII^{+}, F4/80^{+}, CD11b^{+}, Ly6C^{+}, and Ly6G^{+} myeloid cells from the blood of *Lal*$^{-/-}$ mice when a single surface marker was used (Figure 1B). However, further analyses demonstrated that all the CD11c^{-} double gated myeloid subtypes, including CD11b^{+}CD11c^{-}, MHCII^{+}CD11c^{-}, F4/80^{+}CD11c^{-}, Ly6C^{+}CD11c^{-}, and Ly6G^{+}CD11c^{-} cells, showed no increase in PD-L1 expression, while all the CD11c^{+} double gated myeloid subtypes, including CD11b^{+}CD11c^{+}, MHCII^{+}CD11c^{+}, F4/80^{+}CD11c^{+}, Ly6C^{+}CD11c^{+}, and Ly6G^{+}CD11c^{+} cells, showed increased PD-L1 expression in the blood of *Lal*$^{-/-}$ mice vs. *Lal*$^{+/+}$ mice (Figure 1C). An example of PD-L1 expression in CD11b^{+}CD11c^{-} and CD11b^{+}CD11c^{+} cells and their gating strategy are shown in Supplemental Figure 1B. This concludes that LAL deficiency-induced PD-L1 expression was restricted to the CD11c^{+} myeloid subpopulation, whose percentage was increased in the blood of *Lal*$^{-/-}$ mice vs. *Lal*$^{+/+}$ mice (Figure 1D and Supplemental Figure 1C). Flow cytometry analysis also showed up-regulation of MFI of IFNγ, MCP-1, GM-CSF and IL-10 proteins in *Lal*$^{-/-}$ CD11c^{+} cells vs. *Lal*$^{+/+}$ CD11c^{+} cells (Figure 1E). The percentage differences are shown

in Supplemental Figure 1D-E, in which IFNγ, MCP-1, GM-CSF, IL-10, IL-1β and IL-2 showed statistically significant differences. IFNγ has been reported to regulate PD-L1 expression (21). To see whether IFNγ produced by $CD11c^+$ cells is essential for PD-L1 expression, $Lal^{+/+}$ or $Lal^{-/-}$ $CD11c^+$ cells were treated with IFNγ neutralizing antibody or control IgG for 2 days. The percentage of $PD\text{-}L1^+$ cells was decreased in $CD11c^+$ cells with IFNγ neutralizing antibody treatment (Supplemental Figure 1F), suggesting that $CD11c^+$ cells-derived IFNγ participates in regulating PD-L1 expression.

$Lal^{-/-}$ $CD11c^+$ cells suppress T cell proliferation and stimulate tumor growth through PD-L1.

The functions of $Lal^{-/-}$ $CD11c^+$ cells are characterized. First, freshly isolated $Lal^{+/+}$ or $Lal^{-/-}$ $CD11c^+$ blood cells were co-cultured with wild type splenic $CD4^+$ T cells for CFSE proliferation assay in vitro, in which $Lal^{-/-}$ $CD11c^+$ cells drastically suppressed $CD4^+$ T cell proliferation vs. $Lal^{+/+}$ $CD11c^+$ cells (Figure 2A). The in vivo ratios of $CD4^+$ T cells:$CD11c^+$ cells and $CD8^+$ T cells:$CD11c^+$ cells were also greatly decreased in the blood of $Lal^{-/-}$ mice (Figure 2B). To evaluate if the up-regulated PD-L1 expression in $Lal^{-/-}$ $CD11c^+$ cells is responsible for the suppression of T cell proliferation, CFSE-labeled T cells were co-cultured with isolated $Lal^{+/+}$ or $Lal^{-/-}$ $CD11c^+$ cells that were pre-treated with control IgG or anti-PD-L1 antibody. Results showed that blocking PD-L1 with anti-PD-L1 antibody reversed the $Lal^{-/-}$ $CD11c^+$ cells' suppressive activity on T cell proliferation (Figure 2C).

Next, isolated $Lal^{+/+}$ or $Lal^{-/-}$ $CD11c^+$ cells were subcutaneously co-injected with B16 melanoma cells into $Lal^{+/+}$ recipient mice at flank sites. Compared with $Lal^{+/+}$ $CD11c^+$ cells, $Lal^{-/-}$ $CD11c^+$ cells stimulated tumor growth in vivo (Figure 2D). However, after pre-

treated with anti-PD-L1 antibody, *Lal*$^{-/-}$ CD11c^{+} cells' stimulation of tumor growth was reversed (Figure 2E).

Characteristics of *Lal*$^{-/-}$ vs. *Lal*$^{+/+}$ CD11c^{+} cells by scRNA-seq.

Since *Lal*$^{-/-}$ CD11c^{+} cells showed opposite effects (e.g., T cell suppression and tumor stimulation) of normal DCs (e.g., T cell stimulation and tumor suppression), it is important to reveal the intrinsic molecular transition and get a more comprehensive understanding between *Lal*$^{-/-}$ and *Lal*$^{+/+}$ CD11c^{+} cells. scRNA-seq is a powerful technique to clarify heterogeneity of the immune system by identifying novel distinct immune cell subsets and building trajectories for immune cells (22). CD11c^{+} cells were isolated from the blood of *Lal*$^{+/+}$ and *Lal*$^{-/-}$ mice for scRNA-seq analysis. T-stochastic neighbor embedding (tSNE) plot analysis identified two major distinctive cellular clusters of CD11c^{+} cells: 1) clusters 1, 5, 8 (referred to as cluster 158 hereafter) with increased cellular numbers in *Lal*$^{-/-}$ CD11c^{+} cells vs. *Lal*$^{+/+}$ CD11c^{+} cells, and 2) clusters 0, 2, 3, 6 (referred to as cluster 0236 hereafter) with decreased cellular numbers in *Lal*$^{-/-}$ CD11c^{+} cells vs. *Lal*$^{+/+}$ CD11c^{+} cells (Figure 3A). Cluster 158 demonstrated the monocyte feature, while cluster 0236 demonstrated the neutrophil feature (Supplemental Table 1). Interestingly, there were significantly more *Cd274* (gene name of PD-L1) positive cells in cluster 158, and less in cluster 0236 of *Lal*$^{-/-}$ vs. *Lal*$^{+/+}$ CD11c^{+} cells (Figure 3B). There were more *Adgre1*, *Ly6c1*, *Ly6g*, *Ifng*, *Ccl2*, *Csf2* and *Il10* (gene names of F4/80, Ly6C, Ly6G, IFNγ, MCP-1, GM-CSF and IL-10, respectively) positive cell in cluster 158 of *Lal*$^{-/-}$ vs. *Lal*$^{+/+}$ CD11c^{+} cells (Supplemental Figure 2). Other top 50 up-regulated and down-regulated genes in cluster158 and cluster 0236 of *Lal*$^{-/-}$ CD11c^{+} cells can be categorized into three groups,

1) cellular numbers increased in cluster 158 and relatively no change in cluster 0236 (Figure 3C); 2) cellular numbers increased in cluster 158 and decreased in cluster 0236 (Figure 3D); 3) cellular numbers increased in cluster 0236 and no change or increased in cluster 158 (Figure 3E). Log FC, gene expression, and cellular numbers of the top 50 up-regulated and down-regulated genes among all clusters, cluster 158, and cluster 0236 are presented in Supplemental Table 2-7, respectively.

Metabolic reprogramming in *Lal*$^{-/-}$ CD11c^{+} cells.

Metabolic regulation is important to myeloid differentiation and function (23-27). LAL deficiency reduces fatty acid oxidation, which leads to metabolic reprogramming of *Lal*$^{-/-}$ CD11c^{+} cells. Veritably, tSNE plots and pathway analysis of scRNA-seq showed that genes involved in glycolysis and the citrate cycle were up-regulated in *Lal*$^{-/-}$ vs. *Lal*$^{+/+}$ cluster 158 of CD11c^{+} cells (Figure 4A-B and Supplemental Figure 3A-C), which overlap with the increased *Cd274* expression in tSNE plots (Figure 3B). This metabolic reprogramming was associated with ROS over-production (Figure 4C and Supplemental Figure 3D). When expression of genes responding to ROS (selected from the MGI database) was compared between these two clusters, there was a significant shift from cluster 0236 to cluster 158 (Figure 4D). This observation was confirmed by trajectory analysis (Supplemental Figure 3E), in which trajectory dynamic changes and differential lineages were clearly different in cluster 158 and cluster 0236 of *Lal*$^{-/-}$ vs. *Lal*$^{+/+}$ CD11c^{+} cells. Accordingly, scRNA-seq analysis showed up-regulation of *Gsr* gene (encoding for glutathione reductase, an important cellular antioxidant enzyme) in both cluster 158 and cluster 0236 of *Lal*$^{-/-}$ CD11c^{+} cells (Figure 3E and Supplemental Figure 3F). Seahorse

studies showed that both glycolytic metabolism and oxidative phosphorylation (OXPHOS) in mitochondrial respiration were significantly increased in *Lal*$^{-/-}$ vs. *Lal*$^{+/+}$ CD11c^{+} cells by extracellular acidification rate (ECAR) and oxygen consumption rate (OCR) analyses (Figure 4E and Supplemental Figure 4A-B). In addition, *Lal*$^{-/-}$ CD11c^{+} cells demonstrated a higher rate of ATP production than that of *Lal*$^{+/+}$ CD11c^{+} cells (Figure 4F). Protein expression of several key metabolic enzymes in glucose metabolism, including pyruvate dehydrogenase (PDH), glucose-6-phosphate dehydrogenase (G6PD), and lactate dehydrogenase (LDH), were all significantly increased in *Lal*$^{-/-}$ CD11c^{+} cells compared to those in *Lal*$^{+/+}$ CD11c^{+} cells (Figure 4G and Supplemental Figure 4C-D). Additionally, glutamate dehydrogenase (GLUD) in the glutamine pathway showed up-regulation in *Lal*$^{-/-}$ CD11c^{+} cells at the protein level (Figure 4G and Supplemental Figure 4C-D). These results suggest a metabolic switch to glucose and amino acid utilization in *Lal*$^{-/-}$ CD11c^{+} cells.

Interestingly, PD-L1 expression was subjective to metabolic switch regulation, as injection of PDH inhibitor CPI-613 into *Lal*$^{-/-}$ mice reduced the CD11c^{+} cell population, and PD-L1 expression in *Lal*$^{-/-}$ CD11c^{+} cells (Figure 4H). Furthermore, CPI-613 pre-treated *Lal*$^{-/-}$ CD11c^{+} cells showed reduced capabilities in T cell suppression when co-cultured with CD4^{+} T cells in vitro (Figure 4I) and tumor growth stimulation when co-injected with B16 melanoma cells subcutaneously in *Lal*$^{+/+}$ mice (Figure 4J). Clearly, blocking PDH in the glycolysis pathway impaired *Lal*$^{-/-}$ CD11c^{+} cells' immunosuppressive and tumor stimulatory functions. However, CPI-613 treatment in *Lal*$^{-/-}$ CD11c^{+} cells did not change the IFNγ expression level (Supplemental Figure 4E).

CSF1R controls *Lal*$^{-/-}$ CD11c^{+} cells' PD-L1 regulation, T cell suppression and tumor growth stimulation.

In searching for molecular signaling that controls PD-L1 up-regulation in *Lal*$^{-/-}$ CD11c^{+} cells, CSF1R was selected based on scRNA-seq analysis (Figure 3C), as it plays a critical role in myeloid genesis and promotes the differentiation of progenitors into heterogeneous populations of myeloid cells (28, 29). Importantly, tSNE plot analysis of CD11c^{+} cells showed that the number of *Csf1r* gene positive cells was increased in cluster 158 of *Lal*$^{-/-}$ CD11c^{+} blood cells (Figure 3C and 5A), which overlaps with the increased *Cd274* expression (Figure 3B) and the metabolic switch (Figure 4A-B). Flow cytometry analysis confirmed the increased level of CSF1R protein in the *Lal*$^{-/-}$ CD11c^{+} blood cells (Figure 5B and Supplemental Figure 5A). However, this was not the case in *Lal*$^{-/-}$ CD11b^{+}Ly6G^{+} cells (Supplemental Figure 5B), a traditional *Lal*$^{-/-}$ MDSC population that also strongly suppresses T cell proliferation (16, 18, 30) and stimulates tumor growth (17). CSF1R expression was up-regulated in CD11c^{+} myeloid cells from *Lal*$^{-/-}$ mice, including CD11b^{+}CD11c^{+}, Ly6C^{+}CD11c^{+}, Ly6G^{+}CD11c^{+}, MHCⅡ$^{+}$CD11c^{+}, and F4/80^{+}CD11c^{+} cells (Supplemental Figure 5C). To evaluate if the up-regulated CSF1R expression in *Lal*$^{-/-}$ CD11c^{+} cells is responsible for *Lal*$^{-/-}$ CD11c^{+} cell immunosuppressive and tumor stimulatory functions, isolated *Lal*$^{+/+}$ or *Lal*$^{-/-}$ CD11c^{+} cells were pre-treated with control IgG or anti-CSF1R antibody, and then co-cultured with splenic CD4^{+} T cells in vitro or subcutaneously co-injected with B16 melanoma cells in vivo. Results showed that blocking CSF1R reversed *Lal*$^{-/-}$ CD11c^{+} cells' suppressive activity on T cell proliferation (Figure 5C) and impaired stimulation of tumor growth in mice (Figure 5D). Furthermore, treatment of *Lal*$^{-/-}$ mice with anti-CSF1R antibody decreased the percentage and MFI of

PD-L1$^+$ cells in CD11c$^+$ blood cells (Figure 5E and Supplemental Figure 5D), suggesting that the PD-L1 level was regulated by CSF1R. In the T cell suppression study, the source of CSF1R ligand CSF1 came from both CD11c$^+$ and CD4$^+$ T cells. *Lal*$^{-/-}$ CD11c$^+$ cells showed higher CSF1 production than *Lal*$^{+/+}$ CD11c$^+$ cells, while CD4$^+$ T cells showed lower production of CSF1 (Supplemental Figure 5E). However, the IFNγ level was not significantly changed by blocking CSF1R in *Lal*$^{-/-}$ CD11c$^+$ cells (Supplemental Figure 5D). A doxycycline-inducible hLAL myeloid-specific expressing *c-fms*-Tg/KO triple mouse model (18) was used to test if human LAL expression in myeloid cells corrects CSF1R and PD-L1 up-regulation in CD11c$^+$ cells. Indeed, compared to doxycycline-untreated *c-fms*-Tg/KO triple mice (-DOX group), myeloid-specific expression of hLAL (+DOX group) corrected the increased percentages and MFI of CSF1R$^+$, PD-L1$^+$, IFNγ$^+$ and PD-L1$^+$CSF1R$^+$ double positive populations in *Lal*$^{-/-}$ CD11c$^+$ cells, and decreased the percentage of CD11c$^+$ cell population (Figure 5F and Supplemental Figure 5F). Therefore, myeloid expression of human LAL in the humanized model critically controls *Lal*$^{-/-}$ CD11c$^+$ cell homeostasis and pathogenic functions through the CSF1R/PD-L1 axis.

Pharmacological inhibition of LAL up-regulates the expression of CD11c, PD-L1 and CSF1R in murine HD1A myeloid cells and human blood cells.

The above observations were based on the genetic loss of LAL in mice. To confirm these findings by pharmacological inhibition, a LAL-specific inhibitor Lalistat2 (31, 32) was used to treat murine HD1A myeloid cell line that was established previously (33). The LAL enzymatic activity in HD1A myeloid cells was inhibited by Lalistat2 in a dose-dependent fashion (Figure 6A). As Figure 6B and Supplemental Figure 6A shown,

Lalistat2 treatment significantly increased the percentages of $CD11c^+$, $PD\text{-}L1^+$ and $CSF1R^+$ cells in a concentration-dependent fashion in HD1A cells. Western blot analysis further confirmed the up-regulation of PD-L1 in HD1A cells after Lalistat2 treatment (Figure 6C).

To replicate mouse observations in humans, the human blood was collected from healthy subjects and treated with Lalistat2. The expression levels of PD-L1 and CSF1R in $CD11c^+$ cells were gated and analyzed by flow cytometry. As demonstrated in Figure 6D-E and Supplemental Figure 6B, Lalistat2 treatment significantly increased the percentages of $CD11c^+$ cells in the human blood, and the percentages of $PD\text{-}L1^+$ cells and $CSF1R^+$ cells in human blood $CD11c^+$ cells.

Expression of PD-L1, CSF1R and metabolic enzymes in immunosuppressive $CD11c^+$ cells of tumor-bearing mice and cancer patients.

The *Lal*$^{-/-}$ mouse model has a pre-existing condition in favor of tumor growth. To extend the above findings to tumor-induced models (post-tumor injection), B16 melanoma or LLC cells were subcutaneously injected into the flank sites of *Lal*$^{+/+}$ recipient mice in both syngeneic C57BL/6 and allogeneic FVB/N genetic backgrounds for 14 days. The blood was collected from these mice for flow cytometry analysis. As demonstrated in Figure 7A, percentages of $CD11c^+$ cells in the blood were increased in tumor-bearing mice, including B16-injected FVB/N and C57BL/6 mice, and LLC-injected FVB/N and C57BL/6 mice. Both the MFI and percentages of $PD\text{-}L1^+$ cells in $CD11c^+$ cells were up-regulated in the blood of these tumor-bearing mice (Figure 7B and Supplemental Figure 7A-B). Both the MFI and percentages of CSF1R were increased in $CD11c^+$ cells of B16-

injected vs. those of PBS-injected FVB/N mice as well (Figure 7C and Supplemental Figure 7A and 7C). MFI and percentages of metabolic enzyme PDH were significantly increased in $CD11c^+$ cells of B16-injected vs. those of PBS-injected FVB/N mice (Figure 7D and Supplemental Figure 7A and 7D). When co-cultured with $CD4^+$ T splenic cells, $CD11c^+$ cells isolated from the blood of B16-injected mice suppressed T cell proliferation (Figure 7E), demonstrating that they had immunosuppressive functions similar to *Lal*$^{-/-}$ $CD11c^+$ cells. Taken together, tumor-induced mice (post-tumor model) shared characteristics of *Lal*$^{-/-}$ mice (pre-tumor model) by increasing $CD11c^+$ cells with immunosuppressive activity in the blood, in which PD-L1, CSF1R, and glucose metabolic enzyme were upregulated. In addition to these peripheral $CD11c^+$ cells in tumor-bearing mice, Supplemental Figure 7E and 7F showed that the percentages of $CD11c^+$ cells were increased in tumor tissues, accompanied with up-regulated PD-L1 expression. However, the percentages of $CSF1R^+$ cells in these $CD11c^+$ cells were decreased. In *Lal*$^{-/-}$ mice, no increased $CD11c^+$ cells were observed in tumor tissues (Supplemental Figure 7G), probably due to pool exhaustion as the myeloid compartment is already expanded in these mice. In addition, increased PD-L1 expression and decreased CSF1R level were observed in $CD11c^+$ cells of tumor tissues from *Lal*$^{-/-}$ mice (Supplemental Figure 7H).

To explore whether expressions of PD-L1, CSF1R and IFNγ are correlated with CD11c expression in human cancer patients, data mining analyses were performed in human Lung Adenocarcinoma (LUAD), Lung Squamous Cell Carcinoma (LUSC) and Skin Cutaneous Melanoma (SKCM) samples of the TCGA database. Results showed that there were positive correlations between *CD11C* expression vs. *CD274* expression, *CD11c* expression vs. *CSF1R* expression, *CSF1R* expression vs. *CD274* expression,

IFNG expression vs. *CD11c* expression, *IFNG* expression vs. *CD274* expression, and *IFNG* expression vs. *CSF1R* expression in lung cancer and melanoma patients (Figure 7F-H). To confirm these observations, the blood was collected from healthy controls and NSCLC patients with PD-L1 positive scores, and stained with fluorescence-conjugated antibodies for flow cytometry analysis. As Figure 7I demonstrated, the percentages of $CD11c^+$ cells, PD-$L1^+$ cells, and $CSF1R^+$ cells were all increased in the whole blood of NSCLC patients compared to healthy controls. There were more PD-$L1^+$ and $CSF1R^+$ cell populations in gated $CD11c^+$ cells of NSCLC patients than those of healthy controls (Figure 7J and Supplemental Figure 7I). In contrast, within $CD11b^+$HLA-DR^- myeloid cells, there was relatively no change in percentages of PD-$L1^+$ cells or $CSF1R^+$ cells (Supplemental Figure 7I-J). MFI and percentages of metabolic enzyme PDH were significantly increased in $CD11c^+$ cells of NSCLC patients compared to healthy controls (Figure 7K and Supplemental Figure 7K).

Interestingly, data mining analyses of the TCGA database revealed down-regulation of LAL gene expression in various human cancer forms, including Breast Cancer (BRCA), Kidney Chromophobe (KICH), LUAD, LUSC, Pancreatic adenocarcinoma (PAAD), SKCM and Uterine Corpus Endometrial Carcinoma (UCEC) (Figure 7L). LAL levels were further examined in blood $CD11c^+$, PD-$L1^+$, and $CSF1R^+$ cells of NSCLC patients by flow cytometry analysis. Importantly, Figure 7M and Supplemental Figure 7L showed that the LAL levels were decreased not only in the whole blood cells, but also in $CD11c^+$, PD-$L1^+$, and $CSF1R^+$ cells of NSCLC patients compared to healthy controls. Therefore, there is a negative correlation between LAL expression

and expansion of $CD11c^+$, $PD\text{-}L1^+$, and $CSF1R^+$ cells in NSCLC patients, similar to that observed in the *Lal*$^{-/-}$ model and tumor-bearing mice.

Discussion

Anti-tumor immune suppression is a complicated process, which involves both T cell and myeloid cell components in the ecosystem of tumor microenvironment. Among all immune therapies, the PD-L1/PD-1 checkpoint pathway has so far been proven to be a valuable therapeutic target to eradicate malignancies. Engagement of PD-1 by PD-L1 alters the activity of T cells in many ways, including inhibiting T cell proliferation, survival, cytokine production, and other effector functions. In our study, PD-L1 is subjective to neutral lipid regulation that is controlled by LAL. In *Lal*$^{-/-}$ mice, increased PD-L1 expression was observed in whole blood (Figure 1A). Since the *Lal*$^{-/-}$ mouse model provides a favorable environment for tumor growth and metastasis (17), it is intriguing to determine if PD-L1 plays a role in this environment and reveal which immune components contribute to the increase of PD-L1 expression. It is unlikely that increased PD-L1 expression came from the T cell component because *Lal*$^{-/-}$ mice have impaired development and proliferation of T cells (20), which results in extremely low levels of T cells in most immune organs. In contrast, *Lal*$^{-/-}$ mice have robust proliferation of myeloid cells that is initiated in the early stages of myelopoiesis in the bone marrow (16, 18, 30). Therefore, the search for the increased PD-L1 expression was mainly focused on the myeloid lineage of *Lal*$^{-/-}$ mice.

Flow cytometry analysis using various myeloid surface markers revealed that PD-L1 expression was only up-regulated in CD11c^{+} myeloid cells of *Lal*$^{-/-}$ mice (Figure 1B-C). Functionally, isolated *Lal*$^{-/-}$ CD11c^{+} blood cells possessed strong T cell suppression and stimulation of tumor cells (Figure 2), which are two hallmarks of *Lal*$^{-/-}$ MDSCs (16-18). Based on these similarities and standards, *Lal*$^{-/-}$ CD11c^{+} cells are referred to as CD11c^{+}

MDSCs in order to distinguish them from traditional $CD11b^+Ly6G^+$ MDSCs in *Lal*$^{-/-}$ mice. Unlike MDSCs from tumor-bearing mice that are divided into "monocytic" and "granulocytic" MDSCs (34-36), almost all traditional *Lal*$^{-/-}$ MDSCs are $Ly6G^+Ly6C^+$ (18). CD11c is typically considered to be a marker of conventional DCs (11-14), although it has been reported to be expressed on monocytes, granulocytes, macrophages, and a subset of B cells, T cells, and natural killer (NK) cells (37-41). It appears that $CD11c^+$ cells are a highly plastic population with diverse functions in various disease models. These diverse populations were also observed in the *Lal*$^{+/+}$ and *Lal*$^{-/-}$ blood, although most $CD11c^+$ cells possess either neutrophil (cluster 0236) or monocyte (cluster 158) features (Supplemental Table 1).

It is important to distinguish similarities and differences between *Lal*$^{-/-}$ $CD11b^+Ly6G^+$ MDSCs and *Lal*$^{-/-}$ $CD11c^+$ MDSCs at the cellular and molecular levels. In fat catabolism, triglycerides are hydrolyzed to break into fatty acids and glycerol by LAL. Fatty acids are further broken down through the process of beta oxidation (FAO) that results in acetyl-CoA, which can be used in the tricarboxylic acid (TCA) cycle in mitochondria. In the absence of the regular supply of fatty acids during LAL deficiency, cells inevitably use substitutive energy consumption pathways to fuel oxidative phosphorylation (OXPHOS). In *Lal*$^{-/-}$ $CD11b^+Ly6G^+$ MDSCs, Affymetrix GeneChip microarray and Ingenuity Pathway analyses identified the upregulation of many enzymes that are involved in the glycolytic pathway and the TCA cycle. In addition, gene expressions of lactate dehydrogenases, enzymes in the pentose phosphate pathway (energy conservation for biosynthetic purposes), and glycogen synthesis (storage form of glucose and metabolic energy) were up-regulated in *Lal*$^{-/-}$ $CD11b^+Ly6G^+$ MDSCs (42). In

the present study, by using Seahorse analysis for ECAR and OCR measurements, both glycolytic metabolism and OXPHOS in mitochondrial respiration were significantly increased in *Lal*$^{-/-}$ CD11c^{+} MDSCs, accompanied with higher ATP production (Figure 4E-F). scRNA-seq and tSNE clustering approaches showed that genes involved in glycolysis and the TCA cycle were up-regulated in *Lal*$^{-/-}$ CD11c^{+} MDSCs (Figure 4A-B and Supplemental Figure 3A-B). These observations were confirmed by flow cytometry analysis in which protein expression levels of several key glucose downstream metabolic enzymes (PDH, G6PD, LDH) and GLUD were increased in *Lal*$^{-/-}$ CD11c^{+} MDSCs (Figure 4G). During the process of glycolysis, glucose is broken down into pyruvate, which moves into the mitochondria. PDH plays a role in converting pyruvate into acetyl-CoA by decarboxylation to enter TCA cycle in mitochondria. G6PD and LDH control the pentose phosphate pathway and anaerobic glycolysis, respectively. GLUD participates in the glutamine pathway. Taken together, these results suggest a metabolic switch to overuse glucose and amino acids as the energy source in both *Lal*$^{-/-}$ CD11b^{+}Ly6G^{+} MDSCs and *Lal*$^{-/-}$ CD11c^{+} MDSCs. Importantly, inhibition of PDH by CPI-613 pharmacological inhibitor not only reduced the *Lal*$^{-/-}$ CD11c^{+} MDSCs population and their PD-L1 expression (Figure 4H), but also reversed their capabilities in T cell suppression and tumor growth stimulation (Figure 4I-J). Mitochondria help to control various metabolic decision points that determine immune cell functions (43). In *Lal*$^{-/-}$ CD11b^{+}Ly6G^{+} MDSCs, ROS were over-produced and accompanied by damaged mitochondrial function as a penalty of over-using glucose and amino acids (30). A similar observation was observed in *Lal*$^{-/-}$ CD11c^{+} MDSCs. There were major distinctions between gene expression patterns and trajectory lineage differentiation of the ROS pathway in cluster 158 and cluster 0236 of *Lal*$^{-/-}$ CD11c^{+}

MDSCs compared with *Lal*$^{+/+}$ CD11c^{+} cells (Figure 4D and Supplemental Figure 3D-E), which was associated with high level ROS production (Figure 4C). The high level of ROS allows for the stimulation of cell proliferation, induction of genetic instability, and evasion from senescence (44). Accordingly, gene expression of glutathione reductase *Gsr*, a critical enzyme in redox regulation, was up-regulated in *Lal*$^{-/-}$ CD11c^{+} MDSCs (Supplemental Figure 3F). Clearly, both *Lal*$^{-/-}$ CD11b^{+}Ly6G^{+} MDSCs and *Lal*$^{-/-}$ CD11c^{+} MDSCs share a specialized metabolism that differs from their normal counterparts. Metabolic switch and plasticity in the tumor environment compromise immune-mediated tumor destruction, and offer an opportunity to selectively target functions of immune cells for enhancing effective immunotherapy (25, 27).

However, there are significant differences between *Lal*$^{-/-}$ CD11b^{+}Ly6G^{+} MDSCs and *Lal*$^{-/-}$ CD11c^{+} MDSCs. At least two biomarkers (PD-L1, CSF1R) can be used to distinguish *Lal*$^{-/-}$ CD11b^{+}Ly6G^{+} MDSCs and *Lal*$^{-/-}$ CD11c^{+} MDSCs. First, increased PD-L1 expression was only observed in *Lal*$^{-/-}$ CD11c^{+} MDSCs, not in *Lal*$^{-/-}$ CD11b^{+}Ly6G^{+} MDSCs (Figure 1). Pre-treatment with anti-PD-L1 antibody reversed *Lal*$^{-/-}$ CD11c^{+} MDSC suppressive activity of T cells (Figure 2C) and stimulation of tumor growth (Figure 2E). Blockade of PD-L1 on DCs has been reported to enhance T cell activation and cytokine production (10). In murine tumor infiltrating DCs, blockade of PD-L1 also resulted in a better capability to stimulate T cell activation, contributing to a more potent ability to inhibit tumor growth in mice (9, 45). Second, CSF1R expression was increased in cluster 158 of *Lal*$^{-/-}$ CD11c^{+} MDSCs by scRNA-seq and flow cytometry analyses, but not in *Lal*$^{-/-}$ CD11b^{+}Ly6G^{+} MDSCs (Figure 5A-B and Supplemental Figure 5B). Similar to PD-L1, pre-treatment with anti-CSF1R antibody reversed *Lal*$^{-/-}$ CD11c^{+} MDSCs suppressive activity

on T cells (Figure 5C) and stimulation of tumor growth (Figure 5D). These observations in the genetically ablated system were confirmed in murine HD1A myeloid cell line by LAL pharmacological inhibitor Lalistat2 (Figure 6A-C). More importantly, Lalistat2 treatment induced PD-L1 and CSF1R expression in human blood $CD11c^+$ myeloid cells (Figure 6D-E). Therefore, increased PD-L1 and CSF1R expression are the unique features of *Lal*$^{-/-}$ $CD11c^+$ MDSCs that can be used to distinguish them from *Lal*$^{-/-}$ $CD11b^+Ly6G^+$ MDSCs. On the other hand, there was a report showing exclusive overexpression of fatty acid transport protein 2 (FATP2) that was controlled by granulocyte–macrophage colony-stimulating factor through the activation of the STAT5 transcription factor in PMN-MDSCs. Selective inhibition of FATP2 abrogated the activity of PMN-MDSCs and substantially delayed tumor progression (46).

In addition to the increased levels of PD-L1 and CSF1R, *Lal*$^{-/-}$ $CD11c^+$ MDSCs possess many other unique features. The scRNA-seq approach identified that $CD11c^+$ MDSCs could be divided into two major cellular clusters in tSNE clustering analysis (cluster 158 and cluster 0236). Compared with *Lal*$^{+/+}$ $CD11c^+$ cells, *Lal*$^{-/-}$ $CD11c^+$ MDSCs showed increased cellular number in cluster 158 but decreased cellular number in cluster 0236 (Figure 3A). Considering that *Lal*$^{-/-}$ $CD11c^+$ MDSCs possessed immunosuppressive and tumor stimulatory functions instead of DCs' traditional antigen-presenting immune stimulatory function, these two clusters may represent two sub-populations with distinctive functions. It has been reported that DCs switch from an immunostimulatory activation state driving anti-tumor immunity in early-stage tumors to an immunosuppressive activation state at later stages (47). The secretion of immunosuppressive factors by cancer cells has been proposed to be implicated in the

control of DC differentiation, maturation, and function (48). Similarly here, cluster 158 in *Lal*$^{-/-}$ CD11c^{+} MDSCs may contribute to their immunosuppressive and tumor stimulatory functions. Indeed, the gene *Cd274* (PD-L1) level was significantly increased in cluster 158, and slightly decreased in cluster 0236 of *Lal*$^{-/-}$ CD11c^{+} MDSCs compared with *Lal*$^{+/+}$ CD11c^{+} cells (Figure 3B). As demonstrated in Figure 2, *Lal*$^{-/-}$ CD11c^{+} MDSCs exerted their immunosuppressive and tumor stimulatory functions by up-regulating PD-L1 expression. This was controlled by CSF1R, which has a similar gene expression pattern as PD-L1 in cluster 158 and cluster 0236 (Figure 5A). This CSF1R/PD-L1 axis in *Lal*$^{-/-}$ CD11c^{+} MDSCs was at least, in part, responsible for *Lal*$^{-/-}$ CD11c^{+} MDSCs capabilities in suppressing T cells and stimulating tumor growth (Figure 5C-D). As demonstrated in Figure 3C-E and Supplemental Table 2-7, many other genes and pathways may also contribute to functional switch of CD11c^{+} cells in the *Lal*$^{-/-}$ pro-tumor microenvironment. This opens a door for future investigation. For example, flow cytometry analysis showed up-regulation of IFNγ, MCP-1, GM-CSF and IL-10 proteins in *Lal*$^{-/-}$ CD11c^{+} cells vs. *Lal*$^{+/+}$ CD11c^{+} cells (Figure 1E). Among them, IFNγ has been reported to regulate PD-L1 expression (21). Indeed, the percentage of PD-L1^{+} cells was decreased in *Lal*$^{-/-}$ CD11c^{+} cells with IFNγ neutralizing antibody treatment (Supplemental Figure 1F). There were more *Ifng* (gene name of IFNγ) positive cells in cluster 158 of *Lal*$^{-/-}$ vs. *Lal*$^{+/+}$ CD11c^{+} cells (Supplemental Figure 2). Blocking CSF1R did not significantly change the IFNγ level in *Lal*$^{-/-}$ CD11c^{+} cells (Supplemental Figure 5D), suggesting that PD-L1 is regulated by at least two independent pathways in these cells.

Although *Lal*$^{-/-}$ mice are a pre-tumor model, the findings observed in this model can be extended to tumor-bearing models. In both B16 melanoma and LLC tumor-bearing

mice, not only the percentages of $CD11c^+$ cells in the blood were increased, but also expression of PD-L1, CSF1R, and PDH in $CD11c^+$ cells were up-regulated (Figure 7A-D). Functionally, these $CD11c^+$ cells from the B16 melanoma-induced model suppressed T cell proliferation (Figure 7E). Besides, the percentages of $CD11c^+$ cells and the percentages of $PD\text{-}L1^+$ cells in $CD11c^+$ cells were also increased in the tumor tissues of these tumor-bearing mice (Supplemental Figure 7E-F). Thus, tumor-bearing mice shared similar characteristics of *Lal*$^{-/-}$ mice, and $CD11c^+$ MDSC up-regulation is a common feature in both pre-tumor models (*Lal*$^{-/-}$) and post-tumor (tumor-induced) models.

Importantly, when performing the correlation analyses in human cancer patients by data mining of the TCGA database, there were positive correlations among *CD11C*, *CD274*, *CSF1R* and *IFNG* expression in lung adenocarcinoma, lung squamous carcinoma and melanoma (Figure 7F-H). In addition, human NSCLC patients with PD-L1 positive scores confirmed the increased percentages of $CD11c^+$ cells, and increased PD-L1, CSF1R and PDH expression in gated $CD11c^+$ cells from blood (Figure 7I-K). In contrast, increase of PD-L1 or CSF1R expression was not observed in $CD11b^+HLA\text{-}DR^-$ myeloid cells (representing PMN-MDSCs) (Supplemental Figure 7I-J), confirming that the increased expression of PD-L1 and CSF1R was only associated with $CD11c^+$ cells, and less associated with “PMN-MDSCs” in NSCLC patients. Therefore, $CD11c^+$-MDSC upregulation is common in the tumor environment of both tumor-bearing animal models and human cancer patients. This holds a great potential to design $CD11c^+$ cell-based immunotherapy to enhance the efficacy of T cell-based checkpoint immunotherapy for cancer treatment. Recently, there was a report showing that PD-L1 was universally upregulated in tumor-derived $LAMP3^+$ cDCs in almost all human cancer types (49).

Based on the present studies and previous publications, $CD11c^+$ cells seem to possess dual functions depending on genetic defects and existing microenvironments, and can be divided into two subgroups: 1) an anti-tumor subgroup with APC/T cell stimulating/tumor suppressive functions, and 2) a pro-tumor subgroup with T cell suppressive/tumor stimulating functions. The LAL/CSF1R/PD-L1 axis is a major driver in the transition between these two subgroups through neutral lipid to glycolysis metabolic reprogramming.

Last but not least, LIPA expression was down-regulated in multiple forms of human cancers by data mining of the TCGA database (Figure 7L). Flow cytometry analysis further showed down-regulation of LAL in $CD11c^+$, $PD\text{-}L1^+$, and $CSF1R^+$ cells of blood samples from NSCLC patients (Figure 7M). Therefore, observations made from both mouse models (*Lal*$^{-/-}$ and tumor-bearing) and human cancer patients support a notion that LAL plays a suppressive role in these oncogenic processes and can be used for the cancer immunotherapy purpose. LAL (commercial name Kanuma) can be used to treat cancer patients as immunotherapy to decrease pro-tumor immune cells in clinical settings. It is conceivable that LAL negatively promotes CSF1R and PD-L1 at the transcriptional level. LAL is well known for its role to activate nuclear receptors (e.g. PPARs) by generating hormone ligands. How CSF1R and PD-L1 genes are down-regulated by nuclear receptors at the transcriptional level warrants further investigation in the future. It is noticed that several Fos/Jun subunites of AP-1 transcription factor were co-upregulated in cluster 158, but down-regulated in cluster 0236 (Figure 3D). It is intriguing to see the connections between them and regulation of CSF1R and PD-L1 genes as well.

Methods

Animals and cell lines

Wild type (*Lal*$^{+/+}$) and *Lal*$^{-/-}$ mice of the FVB/N and C57BL/6 background were bred inhouse (50, 51). Humanized *c-fms*-rtTA/(TetO)$_7$-CMV-hLAL (*c-fms*-Tg/KO) mice of the FVB/N background are a previously generated triple transgenic mouse model with myeloid-specific doxycycline-inducible expression of wild-type human LAL (hLAL) in *Lal*$^{-/-}$ mice under the control of the *c-fms* promoter (18, 52). Both male and female mice aged three- to four-month-old were used, and all the mice have been backcrossed for more than 10 generations.

The murine B16 melanoma cell line and Lewis lung carcinoma (LLC) cell line (ATCC, Manassas, VA) were cultured in DMEM supplemented with 10% FBS (Gibco) in a 37^{o}C incubator with 5% CO_2. The HD1A myeloid cell line were previously established in our lab (33) and cultured in RPMI 1640 supplemented with 10% FBS in a 33^{o}C incubator with 8% CO_2. To inhibit the LAL activity, HD1A cells were treated with 10 μM, 50 μM, 100 μM or 200 μM LAL inhibitor Lalistat2 (Cayman, Ann Arbor, MI) for 72 h (31, 32). As a control, HD1A cells were treated with DMSO.

Human blood samples

The human blood samples of normal subjects were obtained from Indiana Biobank, and non-small-cell lung cancer (NSCLC at stage III-IV) patients were obtained from Simon Cancer Center Clinic of Indiana University School of Medicine after signing the consent form. NSCLC patients were selected by screening with PD-L1 Tumor Proportion Score (TPS) ≥ 10%. Both normal subjects and NSCLC patients include male and female,

White and African American. To inhibit the LAL activity, human blood cells from normal subjects were removed of red blood cells (RBCs) with lysis buffer (Biolegend, San Diego, CA) and washed with PBS by centrifugation at 240 x g for 5 min at room temperature, and then incubated with 10 μM LAL inhibitor Lalistat2 for 24 h. As a control, human blood cells were incubated with DMSO.

Flow cytometry analysis

Lal$^{+/+}$ and *Lal*$^{-/-}$ mice were euthanized, and the blood was immediately collected from the posterior vena cava. The blood was then treated with RBC lysis buffer to remove RBCs and washed with PBS. For analysis of PD-L1 and CSF1R expression in immune cell subtypes, cells were stained with APC-conjugated anti-CSF1R antibody (AFS98, cat#17-1152-82), APC eFluor 780-conjugated anti-Ly6G antibody (1A8-Ly6g, cat#47-9668-82), and APC eFluor 780-conjugated anti-F4/80 antibody (BM8, cat#47-4801-82), FITC-conjugated anti-CD11b antibody (M1/70, cat#11-0112-82), FITC-conjugated anti-MHCⅡ antibody (M5/114.15.2, cat#11-5321-82), PE-conjugated anti-CD11c antibody (N418, cat#12-0114-82) (eBioscience, San Diego, CA), FITC-conjugated anti-Ly6C antibody (HK1.4, cat#128006), PE-Cy7-conjugated anti-PD-L1 antibody (10F.9G2, cat#124314) (Biolegend) at 4^{o}C for 15 min. Cells were washed with PBS, then were ready for flow cytometry analysis.

For analyses of cytokine and metabolic enzyme levels in CD11c^{+} cells, isolated cells were first stained with PE-conjugated or APC-conjugated (N418, cat#17-0114-82) anti-CD11c antibody at 4^{o}C for 15 min. After being fixed and permeabilized using BD Cytofix/Cytoperm Fixation/Permeabilization Kit (BD Biosciences, San Jose, CA), cells

were incubated with fluorescence conjugated antibodies against intracellular molecules including APC-conjugated anti-IFNγ antibody (XMG1.2, cat#17-7311-82), APC-conjugated anti-IL-2 antibody (JES6-5H4, cat#17-7021-82), APC-conjugated anti-IL-10 antibody (JES5-16E3, cat#17-7101-82), FITC-conjugated anti-GM-CSF antibody (MP1-22E9, cat#17-7331-82), FITC-conjugated anti-IL-1β antibody (NJTEN3, cat#17-7114-80), PE-conjugated anti-MCP-1 antibody (2H5, cat#12-7096-82) (eBioscience), and non-fluorescence conjugated antibodies against metabolic molecules including glucose-6-phosphate dehydrogenase (G6PD) (D5D2, cat#12263S), lactate dehydrogenase (LDH) (C28H7, cat#3558S), pyruvate dehydrogenase (PDH) (cat#2784S), and glutamate dehydrogenase (GLUD) (D9F7P, cat# 12793S) (Cell Signaling, Beverly, MA) at 4°C overnight. On the next day, for non-fluorescence conjugated antibodies, cells were washed and stained with Alexa Fluor 647-conjugated anti-rabbit IgG antibody (cat#4414S) (Cell Signaling) at 4ºC for 30 min, then washed for flow cytometry analysis.

For flow cytometry analysis of human blood samples, the human blood was removed of RBCs and washed with PBS, and then stained with APC-conjugated anti-CSF1R antibody, APC-eFluor 780-conjugated anti-CD11c antibody (3.9, cat#47-0116-42), PE-conjugated anti-PD-L1 antibody (MIH1, cat#12-5983-42), PE-Cy5-conjugated anti-CD11b antibody (ICRF44, cat#15-0118-42), PE-Cy7-conjugated anti-HLA-DR antibody (L243, cat#25-9952-42) (eBioscience) at 4ºC for 15 min. Cells were then washed with PBS, fixed with 1% PFA, and ready for flow cytometry analysis. To analyze LAL levels, cells were further fixed and permeabilized using BD Cytofix/Cytoperm Fixation/Permeabilization Kit, and incubated with non-fluorescence conjugated anti-LAL antibody (53) , at 4°C overnight. On the next day, cells were washed and stained with

FITC-conjugated anti-rabbit IgG antibody at 4°C for 30 min, then washed for flow cytometry analysis.

For flow cytometry analysis, ⩾50,000 cells were acquired and scored using a LSRII machine (mouse samples) or Fortessa (human samples) (BD Biosciences) and calculated based on isotype control. Data were processed using the BD CellQuest Pro software (version 19.f3fcb) and FlowJo (version 10.6.1) (BD Biosciences).

Isolation of blood $CD11c^+$ cells

The blood was collected from the posterior vena cava of mice. After removal of RBCs and PBS wash, cells were first incubated with biotin-conjugated anti-CD11c antibody (N418, cat#130-125-219) (Miltenyi Biotec., Auburn, CA) at 4°C for 30 min. After wash with PBS, cells were then incubated with anti-biotin microbeads at 4°C for another 30 min. Subsequently, cells were subjected to magnetic bead sorting according to the manufacturer's instructions (Miltenyi Biotec.). For blocking antibody treatment, freshly isolated $CD11c^+$ cells were pre-treated with IgG or anti-PD-L1 (5 μg/mL) (10F.9G2, cat#124302, Biolegend) or anti-CSF1R antibodies (5 μg/mL) (AFS98, cat#14-1152-82, eBioscience) or anti-IFNγ (5 μg/mL) (37895, cat#MAB485-100, R&D Systems, Minneapolis, MN) at 4°C for 1 hour, and then co-cultured with $CD4^+$ T cells or co-injected with B16 melanoma cells for further analysis. For CPI-613 treatment, freshly isolated $CD11c^+$ cells were pre-treated with DMSO or 10 μM CPI-613 at 37°C for 30 min, and then co-cultured with $CD4^+$ T cells or co-injected with B16 melanoma cells for further analysis.

T cell proliferation assay

$CD4^+$ T cells were isolated from the spleen and labeled with CFSE as previously described (20). CFSE-labeled $CD4^+$ T cells were then co-cultured with isolated $CD11c^+$ cells in 96-well plates pre-coated with anti-CD3 monoclonal antibody (mAb) (2 μg/mL) (145-2C11, cat#553057) and anti-CD28 mAb (5 μg/mL) (37.51, cat#553295) (BD Biosciences) at 37°C, 5% CO_2 for 4 days. The ratio of $CD11c^+$ cells /$CD4^+$ T cells was 1:1. Proliferation of $CD4^+$ T cells was evaluated as CFSE dilution by flow cytometry analysis.

Subcutaneous injection of tumor cells into *Lal*$^{+/+}$ mice

To study the effects of $CD11c^+$ cells on tumor growth, isolated $CD11c^+$ cells (2×10^5) with or without pre-treatment were mixed with B16 melanoma cells (2×10^5), and the cell mixture was injected subcutaneously at the flank region of *Lal*$^{+/+}$ recipient mice. The tumor growth was monitored twice a week. The tumor volume (mm^3) was estimated by measuring the maximal length (L) and width (W) of a tumor and calculated using the formula: (length × width ^{2})/2.

For tumor-bearing mice experiments, wild type (*Lal*$^{+/+}$) mice of the FVB/N or C57BL/6 background were injected with 1×10^6 B16 melanoma or LLC cells at flank sites on two sides. Fourteen days later, the mice were sacrificed, and the blood was collected for flow cytometry analysis. To analyze the levels of $CD11c^+$, PD-$L1^+$ or $CSF1R^+$ cells in tumors, tumor tissues from B16 melanoma-injected *Lal*$^{+/+}$ or *Lal*$^{-/-}$ FVB/N mice were harvested, digested for single cell preparation, and stained for flow cytometry analysis.

Single-cell RNA sequencing and data analysis

CD11c$^+$ cells were sorted from the blood of *Lal*$^{+/+}$ and *Lal*$^{-/-}$ mice as described above. Briefly, the blood from *Lal*$^{+/+}$ or *Lal*$^{-/-}$ mice was removed of RBCs and washed with PBS twice, and then incubated with anti-CD11c microbeads for magnetic bead sorting. Cells obtained after sorting were washed twice with PBS to remove debris and re-suspended in PBS. To obtain equal amount of cell numbers, cells sorted from 10 *Lal*$^{+/+}$ mice and 4 *Lal*$^{-/-}$ mice were pooled together and mixed well. The number and viability of CD11c$^+$ cells were 1100 cells/μL and >95%, respectively. Immediately after sorting, CD11c$^+$ single cells were run on the 10X Chromium (10X Genomics) and then through library preparation by the Center for Medical Genomics at Indiana University School of Medicine following the recommended protocol for the Chromium Single Cell 3' Reagent Kit. Libraries were run on the NovaSeq S1 for Illumina sequencing.

CellRanger 3.0.2 (http://support.10xgenomics.com/) was utilized to process the raw sequence data generated. CellRanger used bcl2fastq (https://support.illumina.com/) to demultiplex raw base sequence calls generated from the sequencer into sample-specific FASTQ files. The FASTQ files were then aligned to the mouse reference genome mm10 with RNAseq aligner STAR. The aligned reads were traced back to individual cells and the gene expression level of individual genes were quantified based on the number of UMIs (unique molecular indices) detected in each cell. The filtered gene-cell barcode matrices generated by CellRanger were used for further analysis. Cells with unique gene counts over 8000 or having > 10% mitochondrial genes were filtered out. The gene expression was normalized by total expression of the cell, multiplied by a scaling factor 10000, and log2 transformed. Two samples were integrated using FindIntegrationAnchors in Seurat package (54). After scaling the integrated data, the first

13 principle components from principle component analysis (PCA) were used to cluster the cells by a shared nearest neighbor (SNN) modularity optimization based clustering algorithm (55). Clusters were annotated to cell subtypes using SingleR package (56). Visualization was performed with Seurat package. Differential gene expression analysis was analyzed using Wilcoxon Rank Sum test with Seurat package. Trajectory analysis was performed by monocle 2.16.0 (57-59) on ROS response genes (from the Mouse Genome Informatics, or MGI database: http://www.informatics.jax.org/go/term/GO:0000302) using plot_cell_trajectory function after dimensionality reduction with DDRTree algorithm. The accession number is GSE206837.

Pearson correlation analysis of gene expressions of CD11c, PD-L1, CSF1R and IFNγ from the TCGA data base

The Cancer Genome Atlas Lung Adenocarcinoma (TCGA-LUAD) (60) (585 samples), Lung Squamous Carcinoma (TCGA-LUSC) (61) (550 samples), and Skin Cutaneous Melanoma (TCGA-SKCM) (472 samples) data were retrieved from UCSC Xena platform (62), which are in whole or partly based upon data generated by the TCGA Research Network: https://www.cancer.gov/tcga. Normalized gene expression of *CD274*, *CD11C*, *CSF1R* and *IFNG* were compared with each other in the tumor samples. Pearson correlation and its p value were calculated. Expression comparisons of gene *LIPA* (LAL) in Breast Cancer (BRCA), Kidney Chromophobe (KICH), LUAD, LUSC, Pancreatic adenocarcinoma (PAAD), SKCM or Uterine Corpus Endometrial Carcinoma

(UCEC) patients vs. healthy control individuals were also mined from TCGA, including various demographic variable.

ROS Measurement

The reactive oxygen species (ROS) level in $CD11c^+$ cells was measured by flow cytometry as previously described (63). White blood cells from *Lal*$^{+/+}$ and *Lal*$^{-/-}$ mice were collected as described above and stained with PE-conjugated anti-CD11c antibody and 2 μmol/L 2′, 7′-dichlorofluorescein diacetate (Invitrogen, Carlsbad, CA) at 37°C for 30 min. After PBS wash, the ROS level in $CD11c^+$ cells was analyzed using a LSRII machine.

Extracellular acidification rate and oxygen consumption rate (Seahorse) assays.

Extracellular Acidification Rate (ECAR) and Oxygen Consumption Rate (OCR) measurements were performed using a Seahorse Bioscience XF-96 instrument as described previously (64, 65). On the day prior to the experiment, the sensor cartridge was hydrated overnight using the calibration buffer supplied by the manufacturer (Agilent, Santa Clara, CA). On the day of the experiment, $CD11c^+$ cells were freshly isolated as described above, and washed with calibration buffer twice. For ECAR measurement, $CD11c^+$ cells were incubated with glucose-free Seahorse XF base medium supplemented with 2 mM glutamine for 1 h at 37°C in a CO_2 free incubator. The injection ports of the sensors were filled with 20~25 μL of treatment or vehicle in buffer. The sensor was then placed into the XF-96 instrument and calibrated. After calibration, the calibration fluid plate was replaced with the cell plate. The measurement cycle consisted of a 2 min mix, 1 min wait, and a 2 min measurement. Four basal rate measurements were followed by

sequential addition of glucose (100 mM), oligomycin (10 μM), and 2-DG (500 mM) prepared in glucose-free Seahorse XF base medium. Each injection was followed by four measurement cycles.

For OCR measurement, $CD11c^+$ cells were incubated with glucose-free Seahorse XF base medium supplemented with 1 mM pyruvate, 2 mM glutamine, and 10 mM glucose for 1 h at 37°C in a CO_2 free incubator. The following procedure was similar to ECAR measurement, except that four basal rate measurements were followed by sequential addition of oligomycin (100 μM), carbonyl cyanide-4 (trifluoromethoxy) phenylhydrazone (FCCP, 100 μM), and rotenone/antimycin A (50 μM) prepared in glucose-free Seahorse XF base medium. The consumption rates were calculated from the continuous average slope of the decreased O_2 using a compartmentalization model (66). For $CD11c^+$ cells from different genotypes, the rates from 8 wells were used.

LAL activity measurement

The LAL enzymatic activity was determined using 4-methyl-umbelliferyl-oleate (4-MUO) (Sigma, St. Louis, MO) as substrate as described previously (51). Proteins were extracted from HD1A myeloid cells, which have been treated with Lalistat2 or DMSO for 72 hours. Protein concentrations were determined by Pierce™ BCA protein assay kit (Thermo Fisher Scientific, Waltham, MA). Eighteen microgram of protein was added to 0.567 mM substrate solution (0.567 mM 4-MUO, 0.15M sodium acetate/0.01% Tween 80, pH 5.5, 1% (v/v) Triton X-100). Reaction was incubated at 37°C for 30 minutes, and then terminated by adding 100 μL of 0.75 M Tris, pH 8.0. A standard curve was prepared ranging from 0-100 nM 4-methylumbelliferone (4-MU, Sigma). Fluorescence was

measured on a Gemini XPS plate reader (Molecular Devices, San Jose, CA) at 355 nm excitation and 460 nm emission. Data was analyzed using SoftMax program. Assays were linear within the time frame of these assays, and less than 10% of substrate was cleaved. One unit is 1 mmol of 4-MUO cleaved per min under standard assay conditions.

Statistics

Data are expressed as mean ± SD. Differences between two treatment groups were compared by 2-tailed Student's t-test. When more than two groups were compared, one-way ANOVA with post-hoc Newman-Keul's multiple comparison test was used. When the data were entered into a Grouped table with subcolumns, two-way ANONA with multiple comparison test was used. A P value less than 0.05 was considered statistically significant. All analyses were performed with GraphPad Prism 8.4.1 (GraphPad, San Diego, CA).

Study approval

All scientific protocols involving the use of animals have been approved by the Institutional Animal Care and Use Committee of Indiana University School of Medicine and followed guidelines established by the Panel on Euthanasia of the American Veterinary Medical Association. Animals were housed under Institutional Animal Care and Use Committee-approved conditions in a secured animal facility at Indiana University School of Medicine. All protocols involving the use of human blood have been approved by the Institutional Biosafety Committee of Indiana University School of Medicine and the written informed consent was received prior to participation.

Author Contributions

T. Z. designed and performed experiments, analyzed and interpreted the data, and wrote the manuscript. J. W. and S. L. analyzed and interpreted the scRNA-seq data. X. D. performed flow cytometry. E. J. maintained mouse colonies and performed genotyping. N. H. provided the human NSCLC blood samples. K. S., and C. S. are responsible for Seahorse analysis. H. D. and C. Y. designed experiments, analyzed and interpreted the data, and wrote the manuscript.

Acknowledgments

This work was supported by NIH Grant CA225108 (C. Y. and H. D.). The human samples from healthy subjects were made possible with support by the Indiana Biobank and the Indiana Clinical and Translational Sciences Institute, funded in part by UL1TR002529 from the National Institutes of Health, National Center for Advancing Translational Sciences, Clinical and Translational Sciences Award. The bioinformatics analysis and Flow Cytometry Facility were supported by IU Simon Comprehensive Cancer Center, funded in part by NCI Grant P30CA082709.

References

1. Lei X, et al. Immune cells within the tumor microenvironment: Biological functions and roles in cancer immunotherapy. *Cancer Letters.* 2020;470:126-133.
2. Iwai Y, et al. Involvement of PD-L1 on tumor cells in the escape from host immune system and tumor immunotherapy by PD-L1 blockade. *Proceedings of the National Academy of Sciences.* 2002;99(19):12293-12297.
3. Pardoll DM. The blockade of immune checkpoints in cancer immunotherapy. *Nature Reviews Cancer.* 2012;12(4):252-264.
4. Alsaab HO, et al. PD-1 and PD-L1 checkpoint signaling inhibition for cancer immunotherapy: mechanism, combinations, and clinical outcome. *Front Pharmacol.* 2017;8:561.
5. Butte MJ, et al. Programmed death-1 ligand 1 interacts specifically with the B7-1 costimulatory molecule to inhibit T cell responses. *Immunity.* 2007;27(1):111-122.
6. Gupta H, et al. Tumor cell-intrinsic PD-L1 promotes tumor-initiating cell generation and functions in melanoma and ovarian cancer. *Signal Transduction and Targeted Therapy.* 2016;1:16030.
7. Sharma P, Allison JP. Immune checkpoint targeting in cancer therapy: toward combination strategies with curative potential. *Cell.* 2015;161(2):205-214.
8. Zou W, Wolchok JD, Chen L. PD-L1 (B7-H1) and PD-1 pathway blockade for cancer therapy: mechanisms, response biomarkers, and combinations. *Sci Transl Med.* 2016;8(328):328rv4.
9. Curiel TJ, et al. Blockade of B7-H1 improves myeloid dendritic cell–mediated antitumor immunity. *Nature Medicine.* 2003;9(5):562-567.

10. Brown JA, et al. Blockade of programmed death-1 ligands on dendritic cells enhances T cell activation and cytokine production. *The Journal of Immunology.* 2003;170(3):1257-1266.
11. Eisenbarth SC. Dendritic cell subsets in T cell programming: location dictates function. *Nat Rev Immunol.* 2019;19(2):89-103.
12. Wculek SK, et al. Dendritic cells in cancer immunology and immunotherapy. *Nature Reviews Immunology.* 2020;20(1):7-24.
13. Anderson DA, et al. Genetic models of human and mouse dendritic cell development and function. *Nature Reviews Immunology.* 2021;21(2):101-115.
14. Veglia F, Gabrilovich DI. Dendritic cells in cancer: the role revisited. *Curr Opin Immunol.* 2017;45:43-51.
15. Elleder M, et al. Subclinical course of cholesteryl ester storage disease in an adult with hypercholesterolemia, accelerated atherosclerosis, and liver cancer. *Journal of Hepatology.* 2000;32(3):528-534.
16. Qu P, et al. Critical roles of lysosomal acid lipase in myelopoiesis. *Am J Pathol.* 2010;176(5):2394-2404.
17. Zhao T, et al. Activation of mTOR pathway in myeloid-derived suppressor cells stimulates cancer cell proliferation and metastasis in lal(-/-) mice. *Oncogene.* 2015;34(15):1938-1948.
18. Qu P, et al. Myeloid-specific expression of human lysosomal acid lipase corrects malformation and malfunction of myeloid-derived suppressor cells in Lal-/- mice. *J Immunol.* 2011;187(7):3854-3866.

19. Ding X, et al. Lysosomal acid lipase deficiency controls Treg and Breg homeostasis in the lymph nodes of mice with human cancer xenotransplants. *Am J Pathol.* 2021;191(2):353-367.

20. Qu P, et al. Critical roles of lysosomal acid lipase in T cell development and function. *Am J Pathol.* 2009;174(3):944-956.

21. Sun C, Mezzadra R, Schumacher TN. Regulation and function of the PD-L1 checkpoint. *Immunity.* 2018;48(3):434-452.

22. Papalexi E, Satija R. Single-cell RNA sequencing to explore immune cell heterogeneity. *Nat Rev Immunol.* 2018;18(1):35-45.

23. Ganeshan K, Chawla A. Metabolic regulation of immune responses. *Annual Review of Immunology.* 2014;32(1):609-634.

24. He Z, et al. Metabolic regulation of dendritic cell differentiation. *Frontiers in Immunology.* 2019;10:410.

25. O'Sullivan D, et al. Metabolic interventions in the immune response to cancer. *Nature Reviews Immunology.* 2019;19(5):324-335.

26. Buck MD, et al. Metabolic instruction of immunity. *Cell.* 2017;169(4):570-586.

27. Leone RD, Powell JD. Metabolism of immune cells in cancer. *Nature Reviews Cancer.* 2020;20(9):516-531.

28. Stanley ER, Chitu V. CSF-1 receptor signaling in myeloid cells. *Cold Spring Harbor Perspectives in Biology.* 2014;6(6):a021857.

29. Hume DA, MacDonald KP. Therapeutic applications of macrophage colony-stimulating factor-1 (CSF-1) and antagonists of CSF-1 receptor (CSF-1R) signaling. *Blood.* 2012;119(8):1810-1820.

30. Ding X, et al. Critical role of the mTOR pathway in development and function of myeloid-derived suppressor cells in Lal-/- mice. *Am J Pathol.* 2014;184(2):397-408.

31. Grumet L, et al. Lysosomal acid lipase hydrolyzes retinyl ester and affects retinoid turnover. *J Biol Chem.* 2016;291(34):17977-17987.

32. Tuohetahuntila M, et al. Lysosome-mediated degradation of a distinct pool of lipid droplets during hepatic stellate cell activation. *J Biol Chem.* 2017;292(30):12436-12448.

33. Ding X, et al. Establishment of Lal-/- myeloid lineage cell line that resembles myeloid-derived suppressive cells. *PLoS One.* 2015;10(3):e0121001.

34. Gabrilovich DI, Nagaraj S. Myeloid-derived suppressor cells as regulators of the immune system. *Nat Rev Immunol.* 2009;9(3):162-174.

35. Ostrand-Rosenberg S, Sinha P. Myeloid-derived suppressor cells: linking inflammation and cancer. *J Immunol.* 2009;182(8):4499-4506.

36. Sica A, Bronte V. Altered macrophage differentiation and immune dysfunction in tumor development. *J Clin Invest.* 2007;117(5):1155-1166.

37. Golinski M-L, et al. CD11c+ B Cells are mainly memory cells, precursors of antibody secreting cells in healthy donors. *Frontiers in Immunology.* 2020;11:32.

38. Qualai J, et al. Expression of CD11c is associated with unconventional activated T cell subsets with high migratory potential. *PLOS ONE.* 2016;11(4):e0154253.

39. Wouters K, et al. Circulating classical monocytes are associated with CD11c+ macrophages in human visceral adipose tissue. *Scientific Reports.* 2017;7(1):42665.

40. Lewis SM, et al. Expression of CD11c and EMR2 on neutrophils: potential diagnostic biomarkers for sepsis and systemic inflammation. *Clinical & Experimental Immunology.* 2015;182(2):184-194.

41. Aranami T, Miyake S, Yamamura T. Differential expression of CD11c by peripheral blood NK cells reflects temporal activity of multiple sclerosis. *The Journal of Immunology.* 2006;177(8):5659-5667.

42. Yan C, et al. Gene profile of myeloid-derived suppressive cells from the bone marrow of lysosomal acid lipase knock-out mice. *PLoS One.* 2012;7(2):e30701.

43. Mehta MM, Weinberg SE, Chandel NS. Mitochondrial control of immunity: beyond ATP. *Nat Rev Immunol.* 2017;17(10):608-620.

44. Levine AJ, Puzio-Kuter AM. The control of the metabolic switch in cancers by oncogenes and tumor suppressor genes. *Science.* 2010;330(6009):1340-1344.

45. Krempski J, et al. Tumor-infiltrating programmed death receptor-1+ dendritic cells mediate immune suppression in ovarian cancer. *J Immunol.* 2011;186(12):6905-6913.

46. Veglia F, et al. Fatty acid transport protein 2 reprograms neutrophils in cancer. *Nature.* 2019;569(7754):73-78.

47. Scarlett UK, et al. Ovarian cancer progression is controlled by phenotypic changes in dendritic cells. *J Exp Med.* 2012;209(3):495-506.

48. Laoui D, et al. The tumour microenvironment harbours ontogenically distinct dendritic cell populations with opposing effects on tumour immunity. *Nat Commun.* 2016;7:13720.

49. Cheng S, et al. A pan-cancer single-cell transcriptional atlas of tumor infiltrating myeloid cells. *Cell.* 2021;184(3):792-809.

50. Du H, et al. Targeted disruption of the mouse lysosomal acid lipase gene: long-term survival with massive cholesteryl ester and triglyceride storage. *Hum Mol Genet.* 1998;7(9):1347-1354.

51. Du H, et al. Wolman disease/cholesteryl ester storage disease: efficacy of plant-produced human lysosomal acid lipase in mice. *J Lipid Res.* 2008;49(8):1646-1657.

52. Yan C, et al. Macrophage-specific expression of human lysosomal acid lipase corrects inflammation and pathogenic phenotypes in Lal-/- mice. *Am J Pathol.* 2006;169(3):916-926.

53. Du H, Witte DP, Grabowski GA. Tissue and cellular specific expression of murine lysosomal acid lipase mRNA and protein. *J Lipid Res.* 1996;37(5):937-949.

54. Stuart T, et al. Comprehensive integration of single-cell data. *Cell.* 2019;177(7):1888-1902.

55. Waltman L, van Eck NJ. A smart local moving algorithm for large-scale modularity-based community detection. *The European Physical Journal B.* 2013;86(11):471.

56. Aran D, et al. Reference-based analysis of lung single-cell sequencing reveals a transitional profibrotic macrophage. *Nature immunology.* 2019;20(2):163-172.

57. Trapnell C, et al. The dynamics and regulators of cell fate decisions are revealed by pseudotemporal ordering of single cells. *Nature biotechnology.* 2014;32(4):381-386.

58. Qiu X, et al. Single-cell mRNA quantification and differential analysis with Census. *Nature methods.* 2017;14(3):309-315.

59. Qiu X, et al. Reversed graph embedding resolves complex single-cell trajectories. *Nature methods.* 2017;14(10):979-982.

60. TCGA. Comprehensive molecular profiling of lung adenocarcinoma. *Nature.* 2014;511(7511):543-550.

61. TCGA. Comprehensive genomic characterization of squamous cell lung cancers. *Nature.* 2012;489(7417):519-525.

62. Goldman MJ, et al. Visualizing and interpreting cancer genomics data via the Xena platform. *Nat Biotechnol.* 2020;38(6):675-678.

63. Zhao T, et al. Myeloid-derived suppressor cells are involved in lysosomal acid lipase deficiency-induced endothelial cell dysfunctions. *J Immunol.* 2014;193(4):1942-1953.

64. Gordillo GM, et al. Mitochondria as target for tumor management of hemangioendothelioma. *Antioxidants & Redox Signaling.* 2020;34:137-153.

65. Singh K, et al. Epigenetic modification of microRNA-200b contributes to diabetic vasculopathy. *Mol Ther.* 2017;25(12):2689-2704.

66. Mookerjee SA, et al. Quantifying intracellular rates of glycolytic and oxidative ATP production and consumption using extracellular flux measurements. *J Biol Chem.* 2017;292(17):7189-7207.

Figure 1

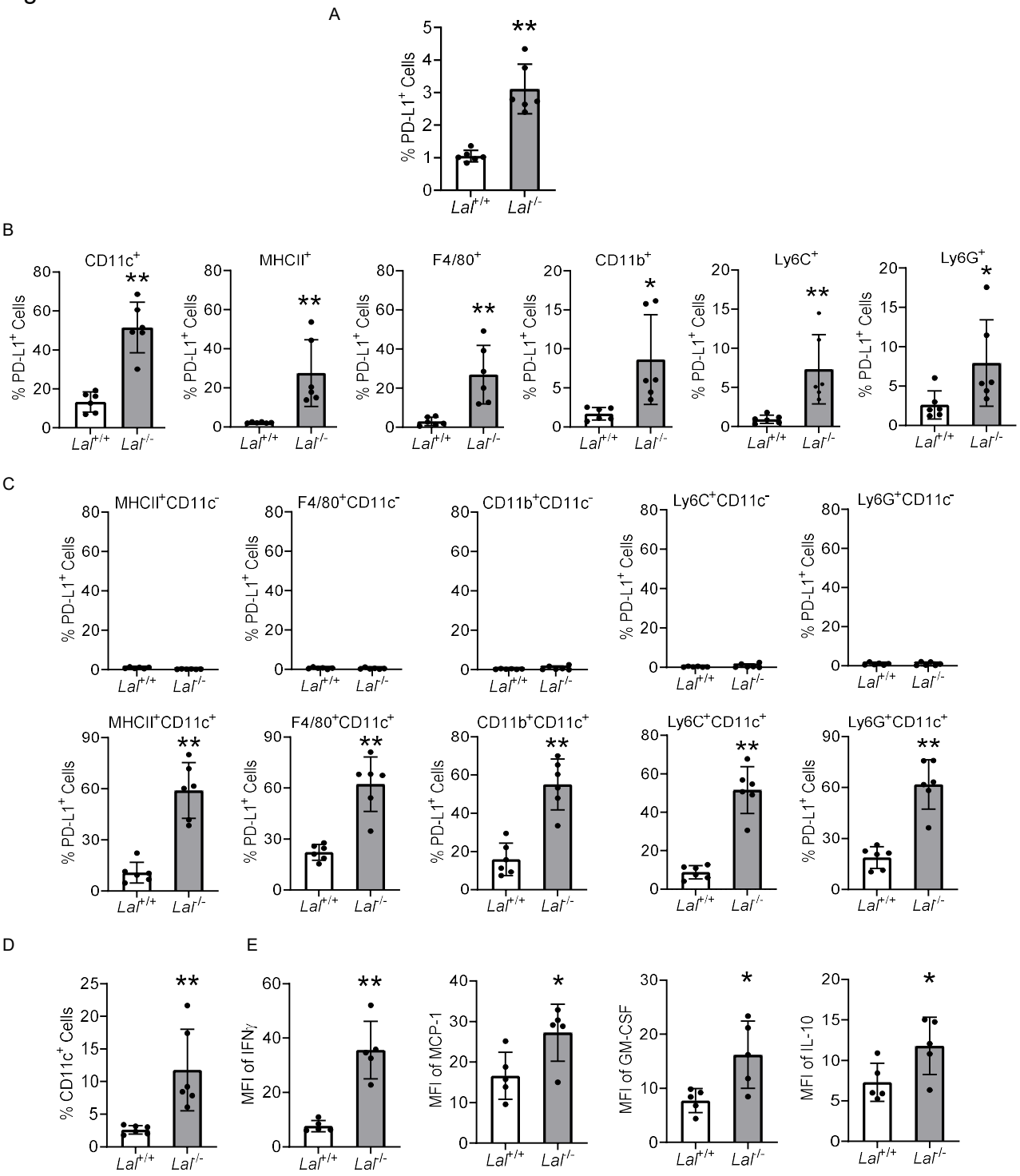
A
% PD-L1+ Cells
Lal+/+
Lal-/-
B
CD11c+
MHCII+
F4/80+
CD11b+
Ly6C+
Ly6G+
C
MHCII+CD11c-
F4/80+CD11c-
CD11b+CD11c-
Ly6C+CD11c-
Ly6G+CD11c-
MHCII+CD11c+
F4/80+CD11c+
CD11b+CD11c+
Ly6C+CD11c+
Ly6G+CD11c+
D
% CD11c+ Cells
E
MFI of IFNγ
MFI of MCP-1
MFI of GM-CSF
MFI of IL-10

Figure 1. PD-L1 expression is increased in *Lal*$^{-/-}$ CD11c^{+} cells. A) Percentage of PD-L1^{+} cells in the blood of *Lal*$^{+/+}$ and *Lal*$^{-/-}$ mice by flow cytometry analysis. **B)** PD-L1 expression in blood CD11c^{+}, MHCII^{+}, F4/80^{+}, CD11b^{+}, Ly6C^{+}, Ly6G^{+} cells of *Lal*$^{-/-}$ vs. *Lal*$^{+/+}$ mice by flow cytometry analysis. **C)** PD-L1 expression in CD11c^{-} or CD11c^{+} double gating myeloid cells of the *Lal*$^{-/-}$ vs. *Lal*$^{+/+}$ blood by flow cytometry analysis. **D)** Percentage of CD11c^{+} cells in the blood of *Lal*$^{+/+}$ and *Lal*$^{-/-}$ mice by flow cytometry analysis. **E)** Cytokine expression in *Lal*$^{-/-}$ vs. *Lal*$^{+/+}$ CD11c^{+} cells by flow cytometry analysis. Data are expressed as mean ± SD; Experiments were independently repeated, n=6 for A-D, n=5 for E. *p<0.05, **p<0.01, unpaired Student's *t* test.

Figure 2

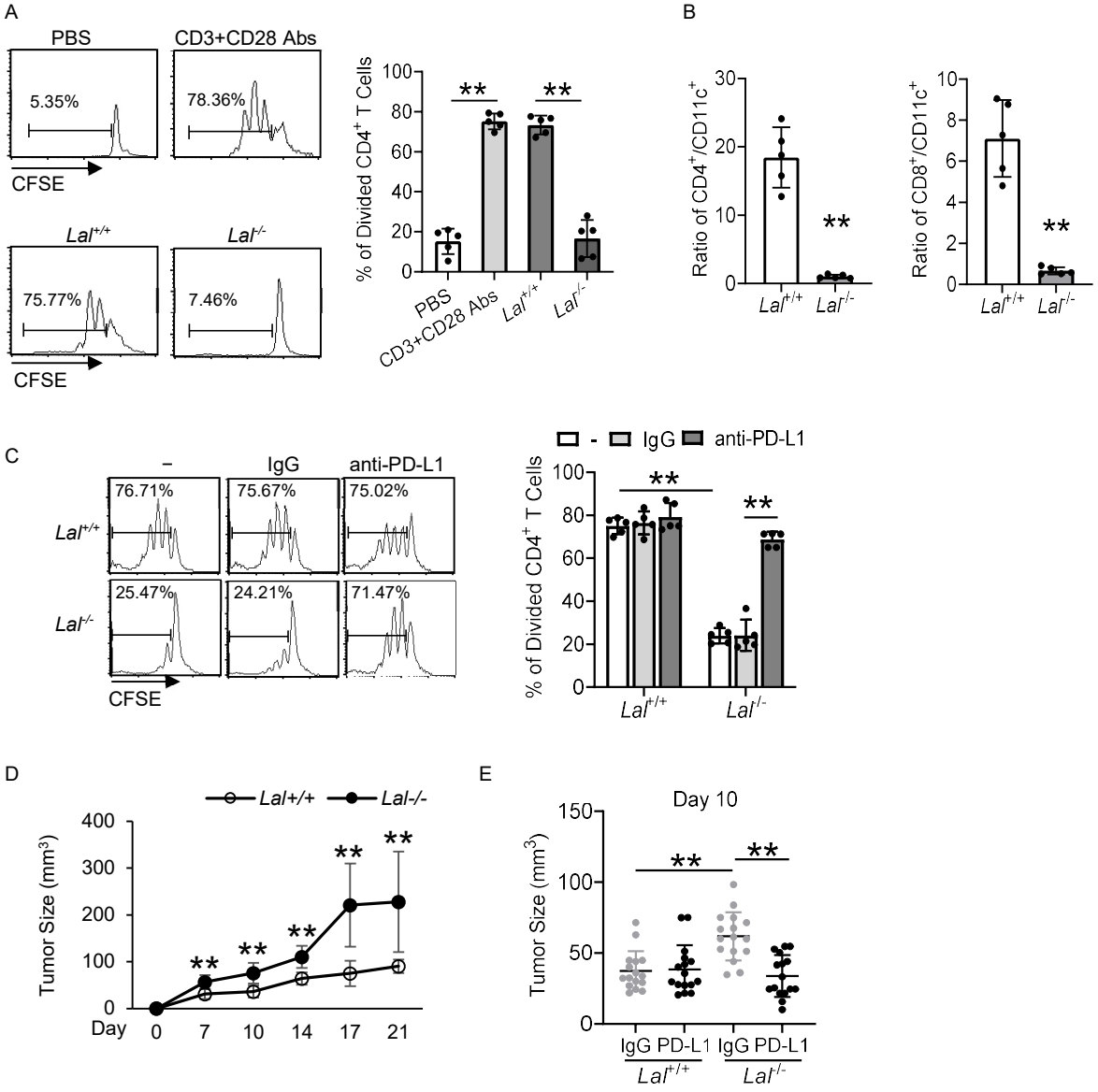
A
PBS
CD3+CD28 Abs
5.35%
78.36%
CFSE
Lal+/+
Lal-/-
75.77%
7.46%
CFSE
% of Divided CD4+ T Cells
PBS
CD3+CD28 Abs
Lal+/+
Lal-/-
B
Ratio of CD4+/CD11c+
Ratio of CD8+/CD11c+
C
–
IgG
anti-PD-L1
76.71%
75.67%
75.02%
25.47%
24.21%
71.47%
CFSE
% of Divided CD4+ T Cells
D
Lal+/+
Lal-/-
Tumor Size (mm3)
Day
E
Day 10
Tumor Size (mm3)
IgG PD-L1 IgG PD-L1

Figure 2. *Lal*$^{-/-}$ CD11c^{+} cells suppress T cell proliferation and stimulate tumor cell growth through PD-L1. A) CFSE-labeled *Lal*$^{+/+}$ CD4^{+} T cells were stimulated with anti-CD3 mAb plus anti-CD28 mAb for 4 days in the presence or absence of *Lal*$^{+/+}$ or *Lal*$^{-/-}$ CD11c^{+} cells at 1:1 ratio between CD4^{+} T cells:CD11c^{+} cells. The proliferation of labeled CD4^{+} T cells was analyzed by flow cytometry. Peaks represent cell division cycles. PBS was used as a negative control. A representative CFSE dilution by flow cytometry is shown on the left. Statistical analyses of % of divided CD4^{+} T cells are on the right. **B)** The ratios of CD4^{+} T cells:CD11c^{+} cells and CD8^{+} T cells:CD11c^{+} cells in the blood of *Lal*$^{-/-}$ vs. *Lal*$^{+/+}$ mice were analyzed by flow cytometry analysis. **C)** Freshly isolated *Lal*$^{+/+}$ or *Lal*$^{-/-}$ CD11c^{+} cells were pre-treated with IgG or anti-PD-L1 antibody (5 μg/mL), and then co-cultured with CFSE-labeled *Lal*$^{+/+}$ CD4^{+} T cells (at 1:1 ratio) for T cell proliferation assay as described in (A). **D)** B16 melanoma cells (2×10^5) were mixed with *Lal*$^{+/+}$ or *Lal*$^{-/-}$ CD11c^{+} cells (2×10^5) and injected subcutaneously at the flank region of *Lal*$^{+/+}$ recipient mice. The tumor size was measured at 7-, 10-, 14-, 17- and 21-days post cell injection and determined using the formula: (length × width^2)/2. **E)** *Lal*$^{+/+}$ or *Lal*$^{-/-}$ CD11c^{+} cells were pre-treated with IgG or anti-PD-L1 antibody (5 μg/mL), and then co-injected with B16 melanoma cells into the flank region of *Lal*$^{+/+}$ recipient mice. Data are expressed as mean ± SD. Experiments were independently repeated, n=5 for A-C, n=10 for D, and n=16 for E. *p<0.05, **p<0.01, 1-way ANOVA for A and E, unpaired Student's *t* test for B and D, 2-way ANOVA for C.

Figure 3

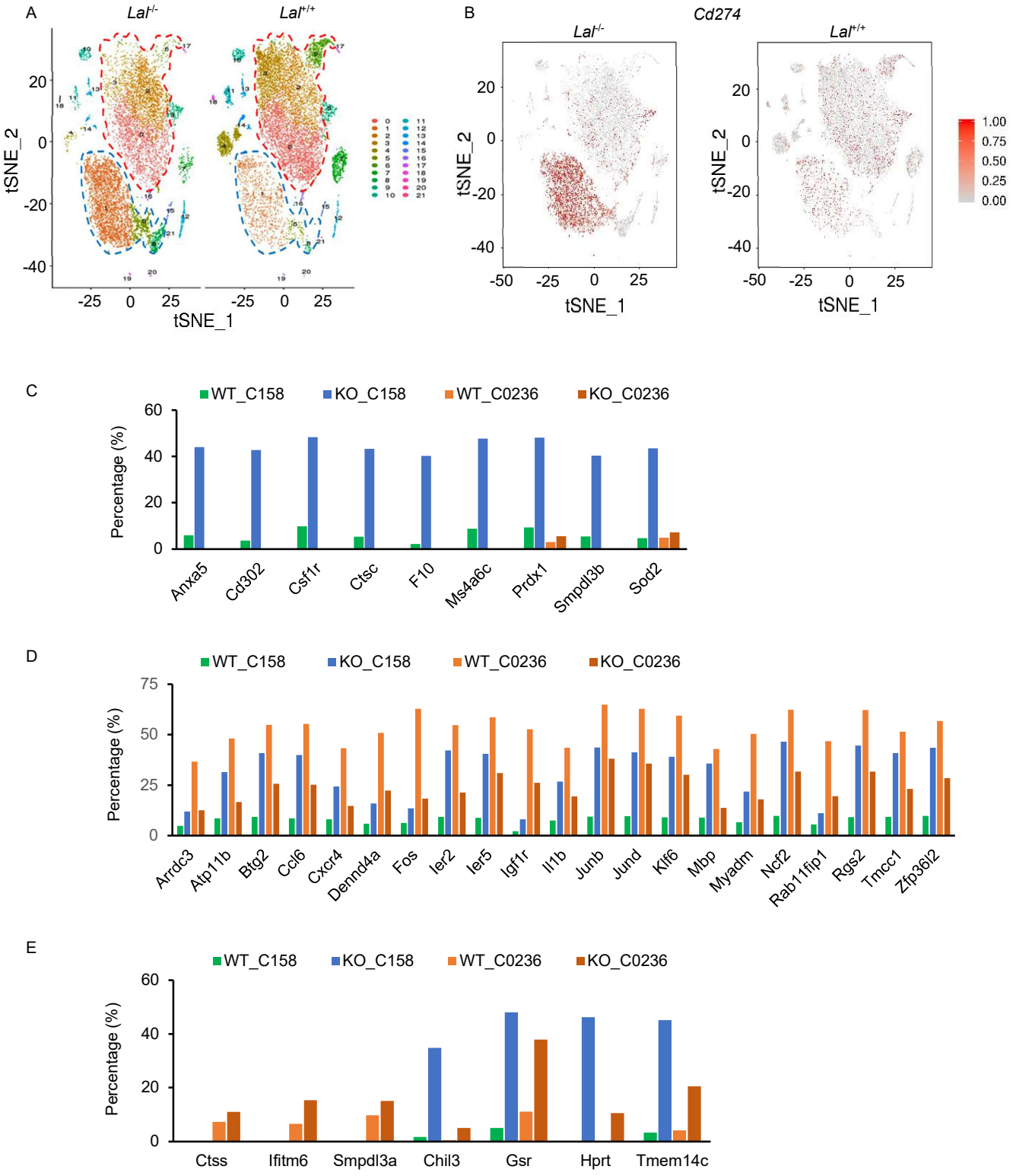
A
Lal-/-
Lal+/+
tSNE_2
tSNE_1
B
Cd274
1.00
0.75
0.50
0.25
0.00
C
WT_C158
KO_C158
WT_C0236
KO_C0236
Percentage (%)
Anxa5
Cd302
Csf1r
Ctsc
F10
Ms4a6c
Prdx1
Smpdl3b
Sod2
D
Arrdc3
Atp11b
Btg2
Ccl6
Cxcr4
Dennd4a
Fos
Ier2
Ier5
Igf1r
Il1b
Junb
Jund
Klf6
Mbp
Myadm
Ncf2
Rab11fip1
Rgs2
Tmcc1
Zfp36l2
E
Ctss
Ifitm6
Smpdl3a
Chil3
Gsr
Hprt
Tmem14c

Figure 3. Identification and gene expression of *Lal*$^{-/-}$ vs*. Lal*$^{+/+}$ CD11c^{+} cell clusters by scRNA-seq. A) tSNE plot of CD11c^{+} cell clusters from *Lal*$^{-/-}$ vs*. Lal*$^{+/+}$ mice. Each dot represents a single cell colored by cluster assignment. The dotted blue line circles cluster 158, and the dotted red line circles cluster 0236. **B)** Feature plot of *Cd274* (PD-L1) expression across cell clusters identified in (A). **C)** Percentages of cells for expressed genes were increased in cluster 158 and relatively unchanged in cluster 0236 of *Lal*$^{-/-}$ vs*. Lal*$^{+/+}$ CD11c^{+} cells. The percentage was calculated using the number of expressed cells for the gene divided by the number of cells for this sample. **D)** Percentages of cells for expressed genes were increased in cluster 158 but decreased in cluster 0236 of *Lal*$^{-/-}$ vs. *Lal*$^{+/+}$ CD11c^{+} cells. **E)** Percentages of cells for expressed genes were increased in cluster 0236 but undetectable or increased in cluster158 of *Lal*$^{-/-}$ vs*. Lal*$^{+/+}$ CD11c^{+} cells.

Figure 4

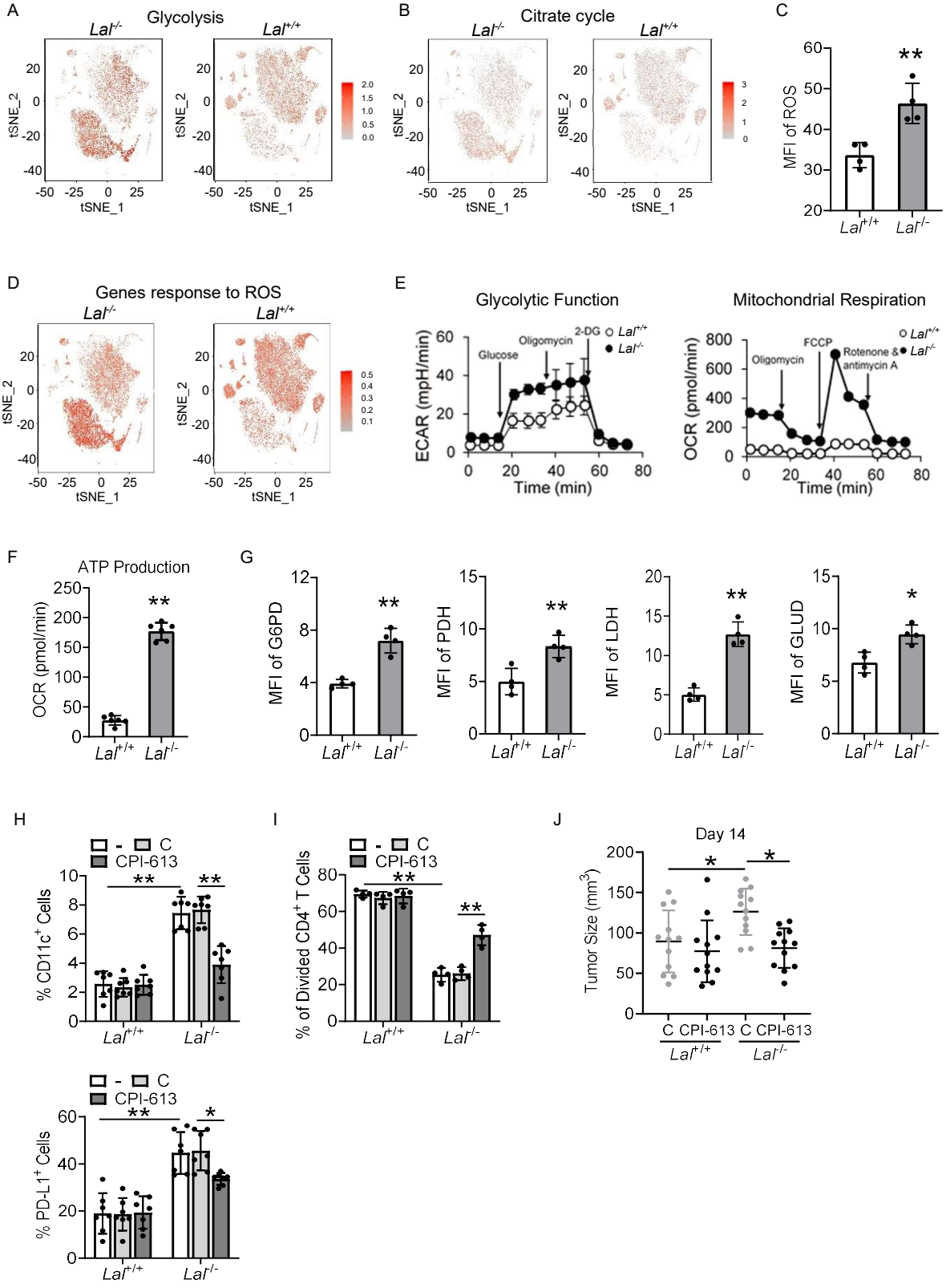
A
Glycolysis
Lal-/-
Lal+/+
tSNE_2
tSNE_1
B
Citrate cycle
C
MFI of ROS
D
Genes response to ROS
E
Glycolytic Function
ECAR (mpH/min)
Glucose
Oligomycin
2-DG
Time (min)
Mitochondrial Respiration
OCR (pmol/min)
FCCP
Rotenone & antimycin A
F
ATP Production
G
MFI of G6PD
MFI of PDH
MFI of LDH
MFI of GLUD
H
- C
CPI-613
% CD11c+ Cells
% PD-L1+ Cells
I
% of Divided CD4+ T Cells
J
Day 14
Tumor Size (mm3)
C CPI-613

Figure 4. Metabolic reprogramming in *Lal*$^{-/-}$ CD11c^{+} cells. Gene expression of **A)** glycolysis and **B)** citrate cycle across cell clusters in tSNE plots of CD11c^{+} cells from *Lal*$^{-/-}$ vs. *Lal*$^{+/+}$ mice. **C)** Statistical analysis of ROS MFI in *Lal*$^{-/-}$ vs. *Lal*$^{+/+}$ CD11c^{+} cells by flow cytometry. **D)** Expression of genes response to ROS across cell clusters in tSNE plots of CD11c^{+} cells from *Lal*$^{-/-}$ vs. *Lal*$^{+/+}$ mice. **E)** ECAR of glycolysis and OCR in mitochondrial respiration in *Lal*$^{-/-}$ vs. *Lal*$^{+/+}$ CD11c^{+} cells. **F)** ATP production in mitochondrial respiration in *Lal*$^{-/-}$ vs. *Lal*$^{+/+}$ CD11c^{+} cells. **G)** MFI of G6PD, PDH, LDH, and GLUD expression in *Lal*$^{-/-}$ vs. *Lal*$^{+/+}$ CD11c^{+} cells by flow cytometry. **H)** The percentage of CD11c^{+} cells in the blood and the percentage of PD-L1^{+} cells in CD11c^{+} blood cells after CPI-613 treatment by flow cytometry analysis. **I)** CPI-613 pre-treated CD11c^{+} cells were co-cultured with CFSE-labeled *Lal*$^{+/+}$ CD4^{+} T cells for T cell proliferation assay. **J)** CPI-613 pre-treated CD11c^{+} cells (2×10^{5}) were co-injected with B16 melanoma cells (2×10^{5}) into the flank region of *Lal*$^{+/+}$ recipient mice for tumor growth assay. Data are expressed as mean ± SD. Experiments were independently repeated, n=4 for C, G and I, n=6-8 for E-F, n=7 for H, and n=12 for J. *p<0.05, **p<0.01, unpaired Student's *t* test for C, F and G, 2-way ANOVA for H and I, 1-way ANOVA for J.

Figure 5

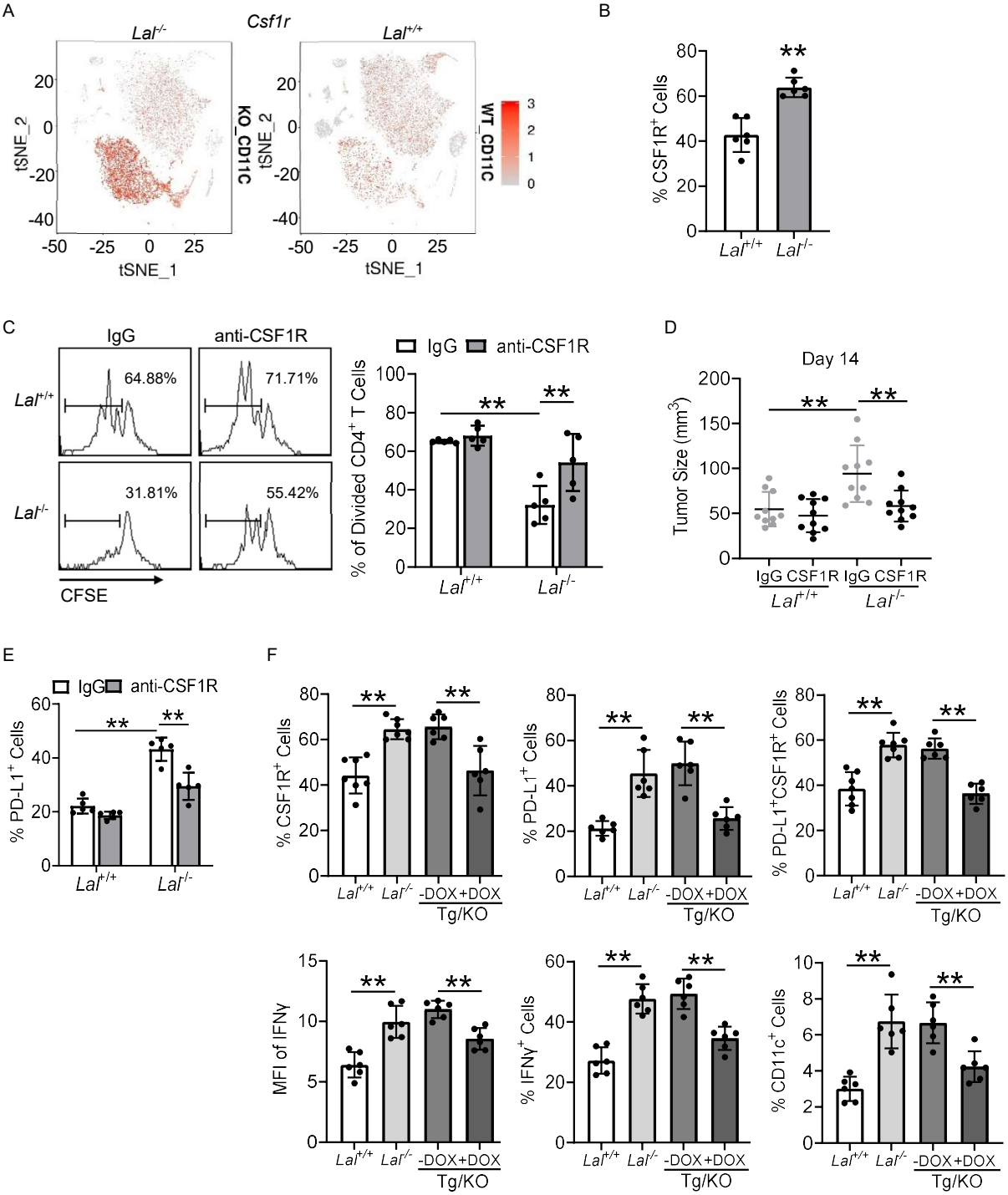
A
Lal-/-
Csf1r
Lal+/+
tSNE_2
tSNE_1
KO_CD11C
WT_CD11C
B
% CSF1R+ Cells
C
IgG
anti-CSF1R
64.88%
71.71%
31.81%
55.42%
CFSE
% of Divided CD4+ T Cells
D
Day 14
Tumor Size (mm3)
IgG CSF1R IgG CSF1R
E
% PD-L1+ Cells
F
% CSF1R+ Cells
% PD-L1+ Cells
% PD-L1+CSF1R+ Cells
MFI of IFNγ
% IFNγ+ Cells
% CD11c+ Cells
-DOX +DOX
Tg/KO

Figure 5. CSF1R expression and function in *Lal*$^{-/-}$ CD11c^{+} cells. A) *Csf1r* expression across cell clusters in tSNE plots of CD11c^{+} cells from *Lal*$^{-/-}$ vs. *Lal*$^{+/+}$ mice. **B)** The percentage of CSF1R^{+} cells in blood CD11c^{+} cells of *Lal*$^{-/-}$ vs. *Lal*$^{+/+}$ mice by flow cytometry analysis. **C)** Isolated *Lal*$^{+/+}$ or *Lal*$^{-/-}$ CD11c^{+} cells were pre-treated with IgG or anti-CSF1R antibody (5 μg/mL), and co-cultured with CFSE-labeled *Lal*$^{+/+}$ CD4^{+} T cells (at 1:1 ratio). The proliferation of labeled CD4^{+} T cells was analyzed by flow cytometry. **D)** Isolated *Lal*$^{+/+}$ or *Lal*$^{-/-}$ CD11c^{+} cells (2×10^{5}) were pre-treated with IgG or anti-CSF1R antibody (5 μg/mL), and co-injected with B16 melanoma cells (2×10^{5}) into the flank region of *Lal*$^{+/+}$ recipient mice. The tumor size was measured at 14 days post cell injection. **E)** The percentage of PD-L1^{+} cells in CD11c^{+} cells after anti-CSF1R antibody treatment (5 μg/mL) by flow cytometry analysis. **F)** The percentages of CSF1R^{+} cells, PD-L1^{+} cells, PD-L1^{+}CSF1R^{+} cells and IFNγ^{+} cells and MFI of IFNγ in blood CD11c^{+} cells, and the percentage of blood CD11c^{+} cells in *Lal*$^{+/+}$, *Lal*$^{-/-}$, untreated (-DOX), and DOX-treated (+DOX) C-fms-Tg/KO (Tg/KO) mice by flow cytometry analysis. Data are expressed as mean ± SD. Experiments were independently repeated, n=6 for B, n=5 for C and E, n=10 for D, and n=6-7 for F. *p<0.05, **p<0.01, unpaired Student's *t* test for B, 2-way ANOVA for C and E, 1-way ANOVA for D and F.

Figure 6

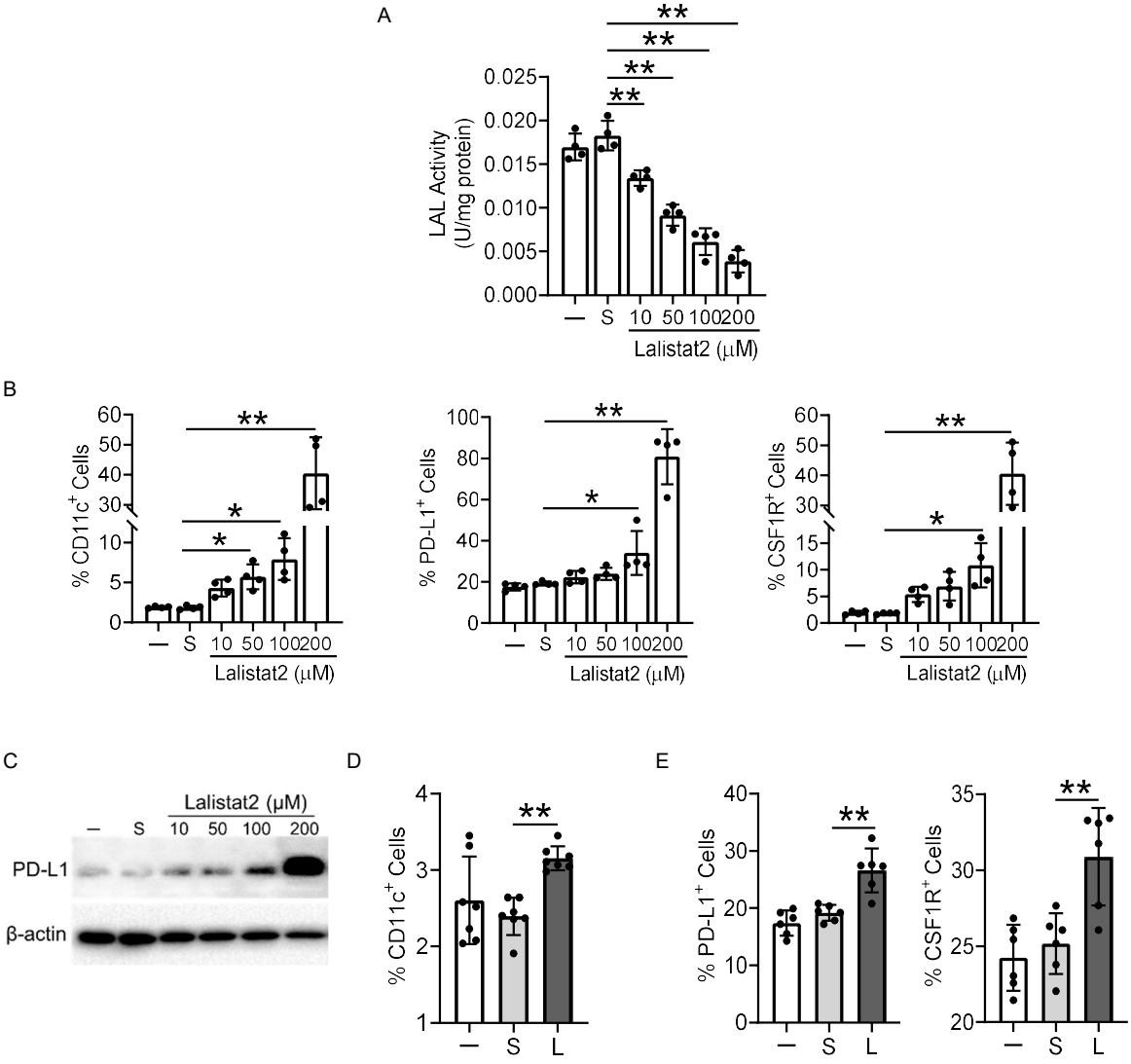
A
LAL Activity (U/mg protein)
0.025
0.020
0.015
0.010
0.005
0.000
**
**
**
**
— S 10 50 100 200
Lalistat2 (μM)
B
% CD11c+ Cells
% PD-L1+ Cells
% CSF1R+ Cells
*
**
Lalistat2 (μM)
C
Lalistat2 (μM)
— S 10 50 100 200
PD-L1
β-actin
D
% CD11c+ Cells
**
— S L
E
% PD-L1+ Cells
% CSF1R+ Cells
**
— S L

Figure 6. Expression of PD-L1 and CSF1R in mouse myeloid cells and human blood CD11c$^+$ cells after Lalistat2 treatment. A) The LAL enzymatic activity in HD1A myeloid cells after incubated with 10 μM, 50 μM, 100 μM, 200 μM Lalistat2, or DMSO (S) for 72 h. **B)** Murine HD1A myeloid cells were incubated with 10 μM, 50 μM, 100 μM, 200 μM Lalistat2, or DMSO (S) for 72 h. The percentages of CD11c$^+$, PD-L1$^+$, and CSF1R$^+$ cells in HD1A myeloid cells were analyzed by flow cytometry. **C)** Expression of PD-L1 in HD1A myeloid cells after Lalistat2 or DMSO treatment for 72 h by Western blot analysis. Representative blots are shown. **D)** Human white blood cells from healthy individuals were incubated with 10 μM Lalistat2 (L) or DMSO (S) for 24 h. The percentages of CD11c$^+$ cells in the whole white blood cells were analyzed by flow cytometry. **E)** Percentages of PD-L1$^+$ and CSF1R$^+$ cells in blood CD11c$^+$ cells of healthy individuals treated with Lalistat2 (L) vs. DMSO (S). Data are expressed as mean ± SD; Experiments were independently repeated, n=4 for A and B, n=3 for C, n=6 for D, n=5 for E. *$p<0.05$, **$p<0.01$, 1-way ANOVA.

Figure 7

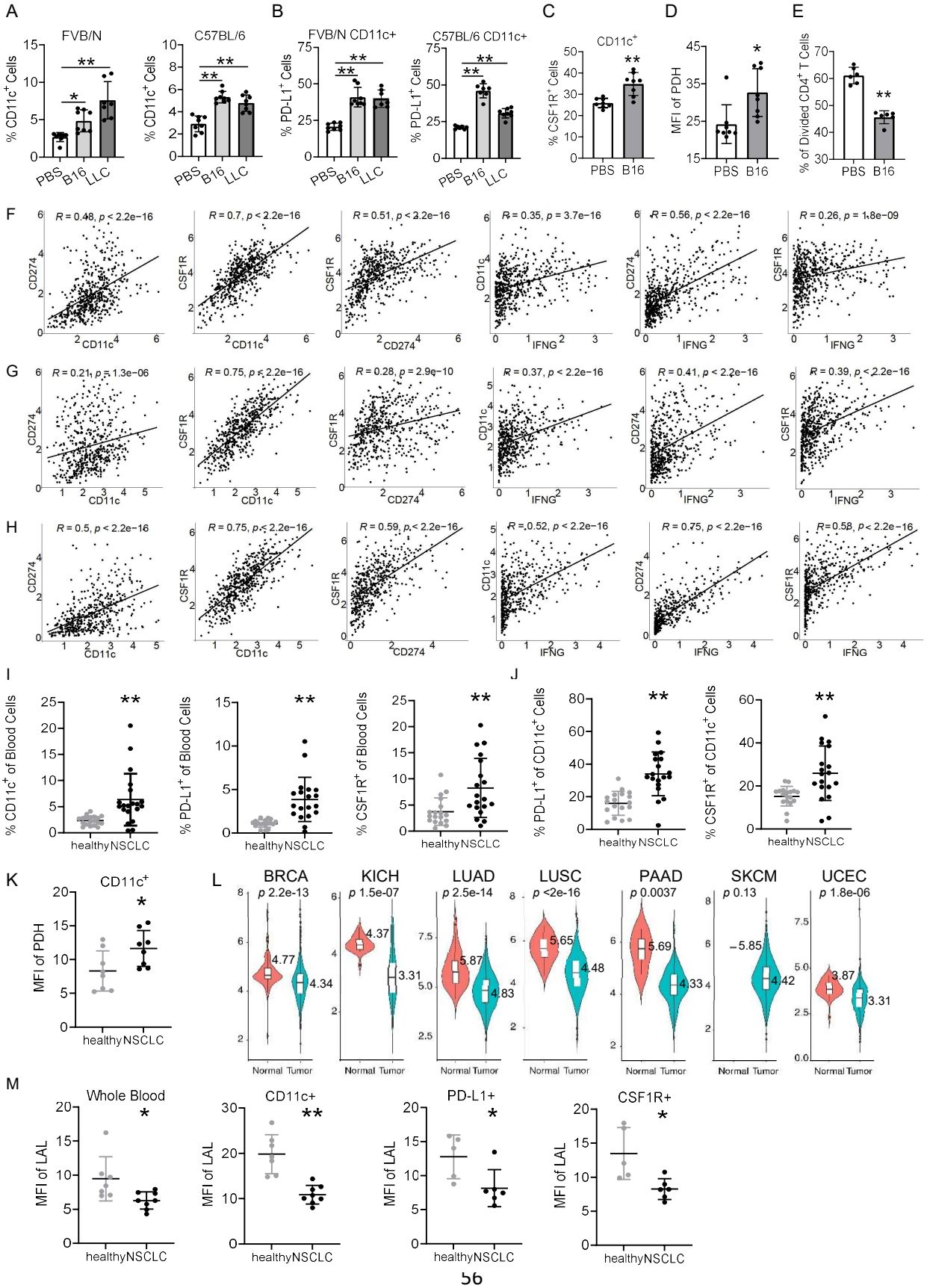
A
FVB/N
C57BL/6
% CD11c+ Cells
PBS B16 LLC
B
FVB/N CD11c+
C57BL/6 CD11c+
% PD-L1+ Cells
C
CD11c+
% CSF1R+ Cells
PBS B16
D
MFI of PDH
E
% of Divided CD4+ T Cells
F
R = 0.48, p < 2.2e−16
R = 0.7, p < 2.2e−16
R = 0.51, p < 2.2e−16
R = 0.35, p = 3.7e−16
R = 0.56, p < 2.2e−16
R = 0.26, p = 1.8e−09
CD274
CSF1R
CD11c
IFNG
G
R = 0.21, p = 1.3e−06
R = 0.75, p < 2.2e−16
R = 0.28, p = 2.9e−10
R = 0.37, p < 2.2e−16
R = 0.41, p < 2.2e−16
R = 0.39, p < 2.2e−16
H
R = 0.5, p < 2.2e−16
R = 0.75, p < 2.2e−16
R = 0.59, p < 2.2e−16
R = 0.52, p < 2.2e−16
R = 0.75, p < 2.2e−16
R = 0.58, p < 2.2e−16
I
% CD11c+ of Blood Cells
% PD-L1+ of Blood Cells
% CSF1R+ of Blood Cells
healthy NSCLC
J
% PD-L1+ of CD11c+ Cells
% CSF1R+ of CD11c+ Cells
K
CD11c+
MFI of PDH
L
BRCA
p 2.2e-13
KICH
p 1.5e-07
LUAD
p 2.5e-14
LUSC
p <2e-16
PAAD
p 0.0037
SKCM
p 0.13
UCEC
p 1.8e-06
4.77
4.34
4.37
3.31
5.87
4.83
5.65
4.48
5.69
4.33
5.85
4.42
3.87
3.31
Normal Tumor
M
Whole Blood
CD11c+
PD-L1+
CSF1R+
MFI of LAL

Figure 7. Expression of PD-L1 and CSF1R in CD11c$^+$ cells of tumor bearing mice and NSCLC patients. A) The percentages of CD11c$^+$ blood cells and **B)** the percentages of PD-L1$^+$ cells in CD11c$^+$ blood cells of B16 melanoma or LLC cell-injected vs. PBS-injected FVB/N or C57BL/6 mice by flow cytometry. **C)** The percentages of CSF1R$^+$ cells in CD11c$^+$ blood cells of B16 melanoma cells-injected vs. PBS-injected FVB/N mice. **D)** MFI of PDH expression in CD11c$^+$ blood cells of B16 melanoma cell-injected vs. PBS-injected FVB/N mice. **E)** CD11c$^+$ blood cells were isolated from B16 melanoma cell-injected or PBS-injected FVB/N mice, and co-cultured with CFSE-labeled *Lal*$^{+/+}$ CD4$^+$ T cells (at 1:1 ratio). The proliferation of labeled CD4$^+$ T cells was analyzed by flow cytometry. **F-H)** Pearson correlation analysis of expressions of *CD11C* and *CD274*, *CD11C* and *CSF1R*, *CD274* and *CSF1R*, *IFNG* and *CD11C*, *IFNG* and *CD274*, *IFNG* and *CSF1R* in samples of LUAD **(F),** LUSC **(G)** and SKCM **(H)**. **I)** Statistical analysis of percentages of CD11c$^+$, PD-L1$^+$, and CSF1R$^+$ cells in the blood of NSCLC patients vs. healthy individuals. **J)** Percentages of PD-L1$^+$ and CSF1R$^+$ cells in blood CD11c$^+$ cells of NSCLC patients vs. healthy individuals. **K)** MFI of PDH expression in blood CD11c$^+$ cells of NSCLC patients vs. healthy individuals. **L)** Expression of gene *LIPA* (LAL) in violin plots from BRCA, KICH, LUAD, LUSC, PAAD, SKCM or UCEC patients vs. healthy individuals. **M)** MFI of LAL in whole blood, CD11c$^+$, PD-L1$^+$, and CSF1R$^+$ cells of NSCLC patients vs. healthy individuals. Data are expressed as mean ± SD; Experiments were independently repeated, n=7-8 for A-D, n=6 for E, n=585 for F, n=550 for G, n=472 for H, n=18-20 for J, n=5-8 for K and M. *p<0.05, **p<0.01, 1-way ANOVA for A and B, unpaired Student's *t* test for C-E, I-K and M.